Stem Cell Reports
Article

OPEN ACCESS

Distinct Neurodegenerative Changes in an Induced Pluripotent Stem Cell Model of Frontotemporal Dementia Linked to Mutant TAU Protein

Marc Ehrlich,[1,2,9] Anna-Lena Hallmann,[1,2,9] Peter Reinhardt,[1,3] Marcos J. Araúzo-Bravo,[1,4,5] Sabrina Korr,[2,6] Albrecht Röpke,[7] Olympia E. Psathaki,[1] Petra Ehling,[6] Sven G. Meuth,[6] Adrian L. Oblak,[8] Jill R. Murrell,[8] Bernardino Ghetti,[8] Holm Zaehres,[1] Hans R. Schöler,[1] Jared Sterneckert,[1,3,10] Tanja Kuhlmann,[2,10] and Gunnar Hargus[1,2,10,*]

[1]Max Planck Institute for Molecular Biomedicine, 48149 Münster, Germany
[2]Institute of Neuropathology, University Hospital Münster, 48149 Münster, Germany
[3]DFG Research Center for Regenerative Therapies, Technische Universität Dresden, 01307 Dresden, Germany
[4]Group of Computational Biology and Systems Biomedicine, Biodonostia Health Research Institute, 20014 San Sebastián, Spain
[5]IKERBASQUE, Basque Foundation for Science, 48011 Bilbao, Spain
[6]Department of Neurology, University of Münster, 48149 Münster, Germany
[7]Institute for Human Genetics, University of Münster, 48149 Münster, Germany
[8]Department of Pathology and Laboratory Medicine, Indiana University, Indianapolis, IN 46202, USA
[9]Co-first author
[10]Co-senior author
*Correspondence: gunnar.hargus@ukmuenster.de
http://dx.doi.org/10.1016/j.stemcr.2015.06.001

SUMMARY

Frontotemporal dementia (FTD) is a frequent form of early-onset dementia and can be caused by mutations in *MAPT* encoding the microtubule-associated protein TAU. Because of limited availability of neural cells from patients' brains, the underlying mechanisms of neurodegeneration in FTD are poorly understood. Here, we derived induced pluripotent stem cells (iPSCs) from individuals with FTD-associated *MAPT* mutations and differentiated them into mature neurons. Patient iPSC-derived neurons demonstrated pronounced TAU pathology with increased fragmentation and phospho-TAU immunoreactivity, decreased neurite extension, and increased but reversible oxidative stress response to inhibition of mitochondrial respiration. Furthermore, FTD neurons showed an activation of the unfolded protein response, and a transcriptome analysis demonstrated distinct, disease-associated gene expression profiles. These findings indicate distinct neurodegenerative changes in FTD caused by mutant TAU and highlight the unique opportunity to use neurons differentiated from patient-specific iPSCs to identify potential targets for drug screening purposes and therapeutic intervention.

INTRODUCTION

Frontotemporal dementia (FTD) comprises a group of neurodegenerative diseases and is the second most common early-onset dementia after Alzheimer's disease (AD), having a prevalence of ~15–22/100,000 person-years (Boxer and Miller, 2005; Knopman and Roberts, 2011). FTD is characterized by cortical degeneration of the frontal and temporal lobes (frontotemporal lobar degeneration [FTLD]) leading to impairment of behavior, language, and cognition (Boxer and Miller, 2005; Goedert et al., 2012). About 20%–30% of patients have hereditary forms of FTD, and up to 15%–20% of these patients carry mutations in the *MAPT* gene located on chromosome 17q21, which encodes the microtubule-associated protein TAU (Goedert and Spillantini, 2011). FTD patients with *MAPT* mutations present with dementia and Parkinson-like motor impairment due to additional degeneration of subcortical brain areas, including the substantia nigra (SN). Thus, this form of FTD was termed FTD and Parkinsonism linked to chromosome 17 (FTDP-17; for review, see Ghetti et al., 2015).

TAU is a neuronal protein that stabilizes microtubules and axoplasmic transport, establishes neuronal polarity, mediates axonal outgrowth and dendritic positioning, and protects DNA from heat damage and oxidative stress (Noble et al., 2013). Six different TAU isoforms are expressed in the adult human brain as a result of alternative splicing of exons 2, 3, and 10 (Goedert et al., 1989). While exons 2 and 3 encode for amino-terminal TAU domains, exon 10 encodes for one of the four microtubule-binding domains in the carboxy-terminal half of TAU (Goedert et al., 1989). In the normal brain, the ratio of isoforms including exon 10 (4R isoforms) to those isoforms devoid of exon 10 (3R isoforms) is usually balanced, but in some FTDP-17 patients, this ratio is shifted toward 4R isoforms, leading to increased deposition of 4R TAU protein within neurons and glial cells (Goedert and Spillantini, 2011).

A pathological hallmark of FTDP-17 is the deposition of excessive amounts of hyperphosphorylated TAU (p-TAU) protein in neurons and glial cells in affected brain areas, including neural cells within the temporal cortex and dopaminergic (DA) neurons of the SN. Hyperphosphorylation of TAU is thought to suppress its ability to stabilize

microtubules, resulting in axonal degeneration and eventual cell death (for review, see Noble et al., 2013). Deposition of p-TAU is not limited to FTD caused by mutant *MAPT* but is seen in about 40%–45% of all FTD patients, grouped together with FTDP-17 as FTLD-TAU, and includes patients with Pick's disease, progressive supranuclear palsy (PSP), and corticobasal degeneration (Goedert et al., 2012; Irwin et al., 2015). Furthermore, excessive accumulation of p-TAU is found in patients with AD, which together with FTLD-TAU forms the large group of neurodegenerative tauopathies.

Despite thorough characterization of histopathological hallmarks in FTDP-17, mechanisms leading to neuronal degeneration remain largely elusive. This originates, at least in part, from the limited availability of viable neurons from patients' brains. In this context, induced pluripotent stem cells (iPSCs) uniquely enable the identification of mechanisms of disease development in patient-derived neurons. As such, iPSCs have been widely used to study neurodegenerative changes in a variety of neurodegenerative disorders such as Parkinson's disease (PD), AD, or FTD caused by mutant *GRN* or mutant *C9ORF72* (Almeida et al., 2012, 2013; Cooper et al., 2012; Hargus et al., 2010; Reinhardt et al., 2013b; Soldner et al., 2009; for review, see Hargus et al., 2014b). Here, we generated iPSCs from individuals with *MAPT* mutations as an in vitro model of FTDP-17 to identify distinct neurodegenerative changes in FTDP-17.

RESULTS

Derivation and Characterization of iPSCs

We derived iPSCs from individuals carrying the N279K *MAPT* mutation (referred to as FTDP-17-1) or the V337M *MAPT* mutation (referred to as FTDP-17-2), located in exons 10 and 12, respectively. iPSCs were generated by lentiviral transduction of fibroblasts with a polycistronic vector encoding *OCT4*, *KLF4*, *SOX2*, and *C-MYC*. The same procedure was applied to derive iPSCs from two healthy individuals (Ctrl-1 and Ctrl-2). An additional control iPSC line was also included in this study (Ctrl-3), which had been generated with the same four transcription factors (Reinhardt et al., 2013b). Altogether, four FTDP-17 iPSC clones (FTDP-17-1-I, FTDP-17-1-II, FTDP-17-2-I, and FTDP-17-2-II) and four Ctrl-iPSC clones (Ctrl-1-I, Ctrl-1-II, Ctrl-2-I, and Ctrl-3-I) were used in this study. Undifferentiated iPSCs expressed the pluripotency-associated markers OCT4, NANOG, SSEA-4, TRA 1-60, and TRA 1-81 (Figure 1A) and expressed *OCT4*, *KLF4*, *SOX2*, and *C-MYC* at levels comparable to those in H9 embryonic stem cells (ESCs) (Figure 1B). Sanger sequencing confirmed the N279K and the V337M *MAPT* mutation in FTDP-17-patient-derived stem cells (Figures 1C and 1D). Furthermore, we performed whole-genome microarray analysis on undifferentiated Ctrl- and FTDP-17 iPSCs (Figure 1E). This analysis revealed comparable expression profiles in all iPSC clones, which were similar to those of ESCs, but clearly differed from those of fibroblasts (Figure 1E). FTDP-17 and Ctrl cells carried normal karyotypes (Figure 1F), and teratoma formation assays confirmed pluripotency of iPSCs, which differentiated into mesodermal, endodermal, and ectodermal derivatives in vivo (Figure 1G).

Neuronal Differentiation Is Not Impaired in FTDP-17 iPSCs

We have recently developed a protocol to efficiently generate neural progenitor cells and mature neurons from human pluripotent stem cells (Hargus et al., 2014a; Reinhardt et al., 2013a). Using this protocol, we observed efficient derivation of NESTIN$^+$ and SOX1$^+$ neural progenitor cells from both Ctrl- and FTDP-17 iPSCs (Figure 2A). Progenitor cells from both groups subsequently differentiated at similar efficiencies into mature βIII-TUBULIN$^+$ neurons (Figure 2B). Approximately 45% of these neurons were γ-aminobutyric acid$^+$ GABAergic neurons (Figures S1A and S1B), and about 50% were midbrain-like FOXA2$^+$ and tyrosine hydroxylase$^+$ (TH$^+$) DA neurons, which are at significant risk in FTDP-17 (Figures 2B–2E; Slowinski et al., 2007); 2%–4% of all neurons were choline acetyltransferase$^+$ cholinergic neurons (Figures S1C and S1D). To further characterize maturation of iPSC-derived neurons, we obtained electrophysiological recordings using the patch-clamp technique. Both Ctrl- and FTDP-17 neurons fired evoked action potentials with no obvious differences in size, shape, and amplitude (Figure 2F). Furthermore, whole cell voltage-clamp currents and tetrodotoxin (TTX) sensitivity of action potentials indicated functional voltage-gated Na$^+$ channel inward currents in both Ctrl and FTDP-17 iPSC-derived neurons (Figure 2F). These data demonstrated proper maturation of iPSC-derived neurons in vitro and indicated that neuronal differentiation is not impaired in FTDP-17 iPSCs.

Altered Expression of TAU in FTDP-17 iPSC-Derived Neurons

As mutant *MAPT* causes FTDP-17, we next set out to investigate whether FTDP-17 neurons exhibit altered expression of TAU on mRNA and protein levels. Thus, we first performed qPCR analysis for total *TAU* and for different *TAU* isoforms in differentiated Ctrl and FTDP-17 iPSCs (Figures 3A–3C and S2A). An analysis of total *TAU* expression revealed varying expression levels among the different iPSC clones but no significant differences between the Ctrl and FTDP-17 group (Figure 3A). Similarly, expression levels

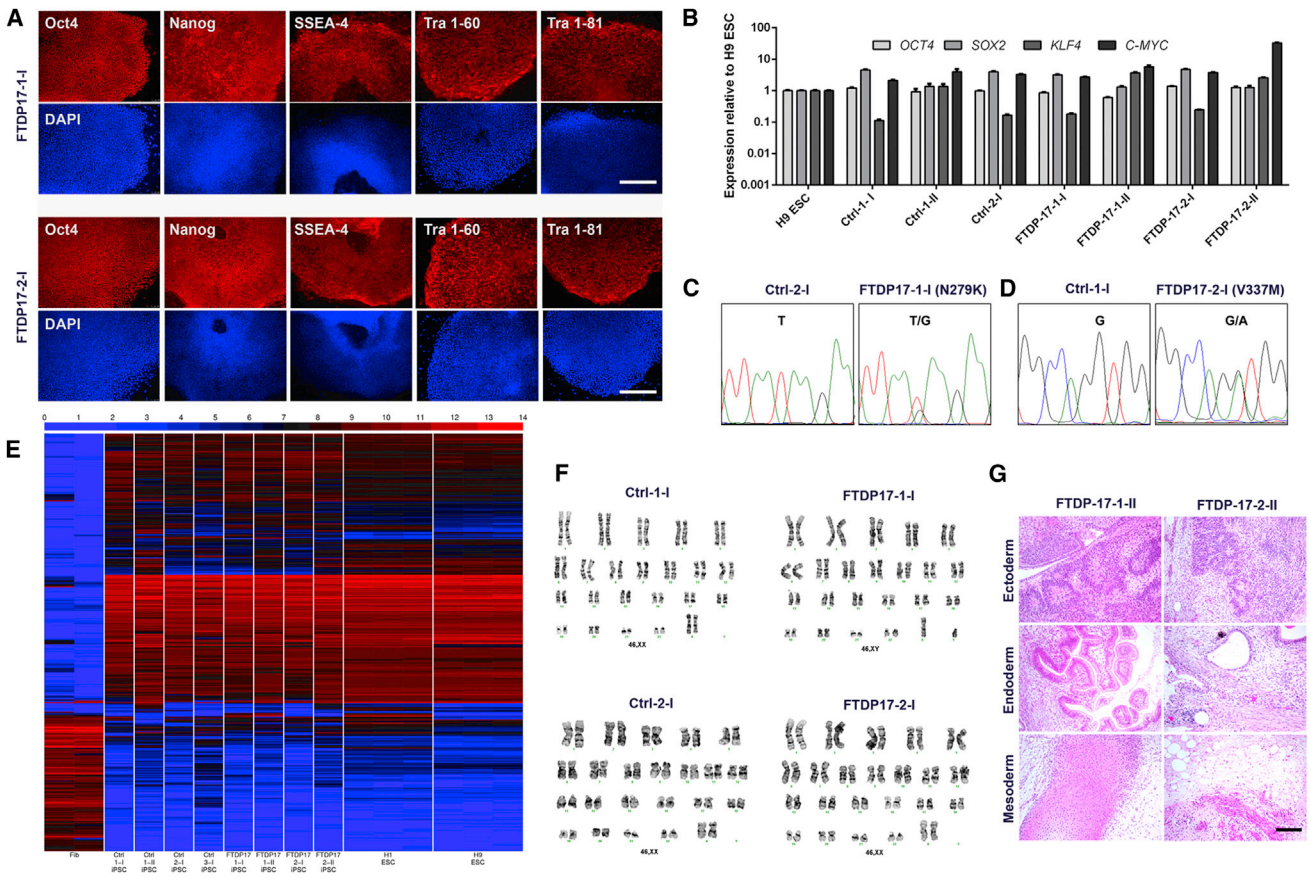

Figure 1. Derivation and Characterization of Ctrl and FTDP-17 iPSCs

(A) Immunostainings of FTDP-17-1 and FTDP-17-2 iPSCs demonstrating expression of pluripotency-associated markers. Scale bars represent 400 μm.

(B) qRT-PCR expression analysis of endogenous *OCT4*, *SOX2*, *KLF4*, and *C-MYC* in iPSC clones and H9 ESCs. Data are represented as mean of three replicates +SEM.

(C and D) DNA sequencing electropherograms from genomic DNA of differentiated Ctrl-1-I, Ctrl-2-I, FTDP-17-I-1, and FTDP-17-2-I iPSCs confirming the presence of the heterozygous N279K *MAPT* mutation in exon 10 in FTDP-17-1 cells and the heterozygous V337M *MAPT* mutation in exon 12 in FTDP-17-2 cells.

(E) Heatmap demonstrating whole-genome expression profiles of human fibroblasts (Fib), of undifferentiated Ctrl and FTDP-17 iPSCs, and of H1 and H9 ESCs.

(F) G-banded karyotype analysis of differentiated Ctrl and FTDP-17 iPSCs.

(G) H&E stainings of teratoma showing differentiation of FTDP-17-1 and FTDP-17-2 iPSCs into mesoderm, endoderm, and ectoderm in vivo. The scale bar represents 200 μm.

of *TAU* isoforms, including exon 2, did not differ between Ctrl and FTDP-17 neurons (Figure 3B). Isoforms containing exon 3 were not detected in any of the cultures. However, we observed mutation-specific differences in the expression of 4R *TAU* isoforms, which include exon 10 (Figures 3C, 3D, and S2A). FTDP-17-1-I/II neurons carrying the N279K mutation expressed significantly higher levels of 4R *TAU*, in contrast to FTDP-17-2-I/II neurons carrying the V337M mutation, which showed 4R *TAU* expression levels comparable to Ctrl neurons. This observation was important for the validation of our iPSC model of FTDP-17 since in brains of FTDP-17 patients, some *MAPT* mutations, including the N279K mutation, lead to missplicing of *MAPT* with an increased expression of 4R *TAU*, while others, including the V337M mutation, do not (Goedert and Spillantini, 2011).

Next, we investigated the expression of TAU protein in Ctrl and FTDP-17 neurons by western blotting (Figures 3E–3K). By using the HT7 TAU antibody, we observed a band of around 52 kDA in both Ctrl- and FTDP-17 neurons, reflecting predominant expression of fetal TAU, as previously described for in vitro-differentiated human

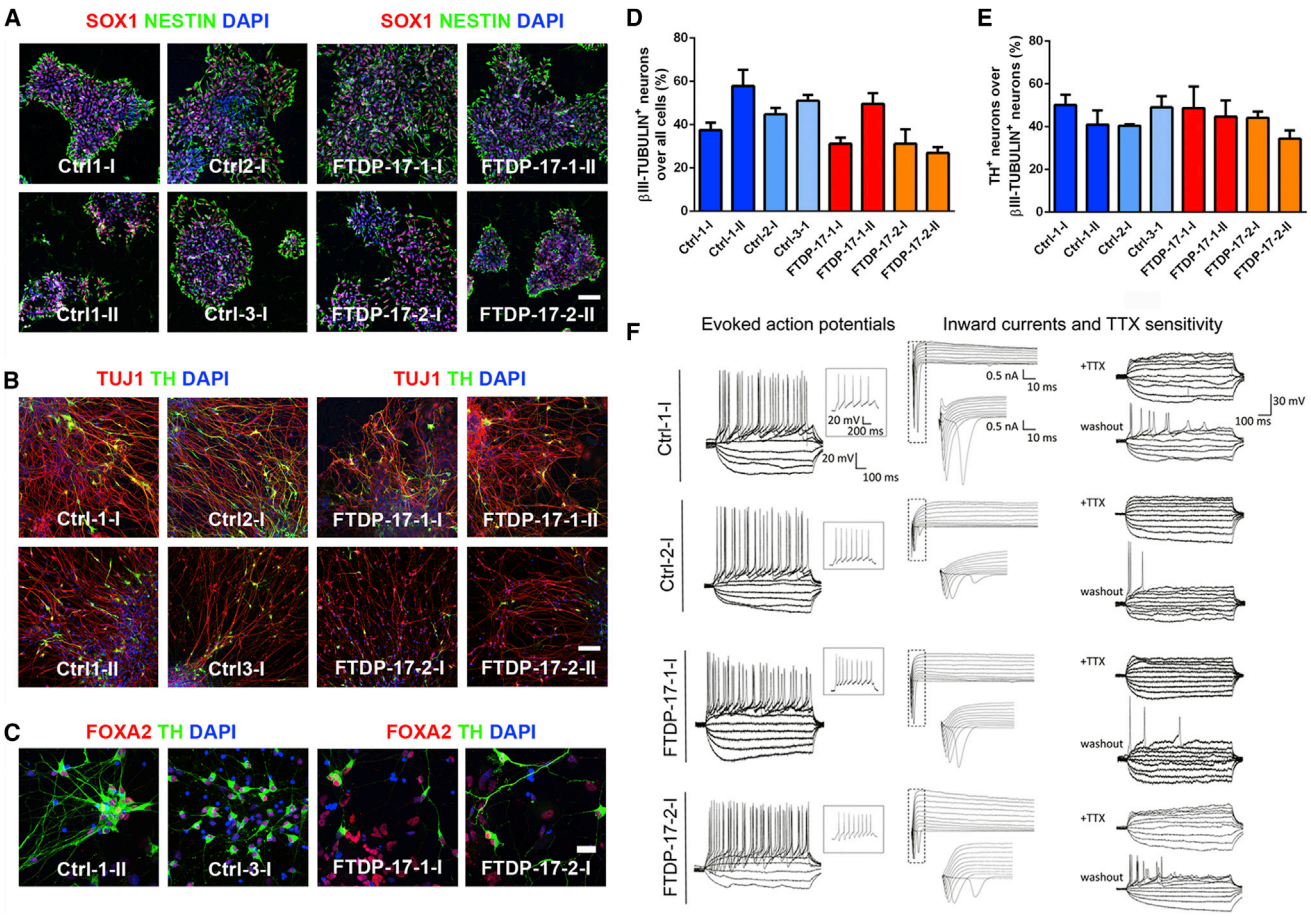

Figure 2. Differentiation of Ctrl and FTDP-17 iPSCs into Mature Neurons

(A) Immunostainings for SOX1 (red) and NESTIN (green) demonstrating differentiation of Ctrl and FTDP-17 iPSCs into neural progenitor cells. Nuclei were counterstained with DAPI (blue). The scale bar represents 50 μm.

(B and C) Immunostainings for (B) TUJ1 (βIII-TUBULIN, red) and TH (green) as well as (C) for FOXA2 (red) and TH (green) showing differentiation of Ctrl and FTDP-17 iPSCs into mature midbrain-like DA neurons. Nuclei were counterstained with DAPI (blue). Scale bars represent 50 μm in (B) and 10 μm in (C).

(D and E) Quantification of immunostainings for (D) βIII-TUBULIN and (E) TH. Data are represented as mean of replicates from three independent differentiation experiments +SEM.

(F) Representative traces of evoked action potentials during current-clamp recordings of Ctrl and FTDP-17 neurons with inserts depicting single action potentials at −30 mV (n = 7; left). Whole-cell voltage-clamp currents (n = 7; middle) and TTX sensitivity of action potentials (n = 5; right) indicate functional voltage-gated Na^+ channel inward currents. The indicated scales apply to the complete panel. All recordings were performed on cells from one differentiation experiment per line.

See also Figure S1.

ESC-derived neurons (Iovino et al., 2010). Furthermore, we identified TAU fragments with a size of 25–27 kDa, which were only weakly expressed in Ctrl neurons but strongly expressed in FTDP-17 neurons (Figure 3E). Thus, it is possible that the N279K and the V337M *MAPT* mutations result in increased fragmentation of full-length TAU protein, as previously described for the A152T *MAPT* variant in differentiated neurons (Fong et al., 2013). To address this possibility, we quantified full-length TAU and fragments in Ctrl and FTDP-17 neurons and found increased amounts of TAU fragments in FTDP-17-1-I/II and FTDP-17-2-I/II neurons at the expense of full-length TAU (Figures 3F and 3G). These findings of increased TAU fragmentation were reproduced using three different TAU antibodies directed against the central core (TAU-5; Figures 3H and 3I), the C terminus (TAU-C17; Figures S2B and S2C), and the N terminus of TAU (TAU-A12; Figures S2D and S2E) as well as with an antibody that specifically recognizes CASPASE-cleaved TAU (TAU-C3; Figures 3J and 3K).

Next, we performed immunostainings on Ctrl and FTDP-17 neurons using the AT8 antibody, which detects p-TAU (Figures 3L–3O). In comparison to Ctrl cultures, we observed significantly increased numbers of $AT8^+/TH^+$ neurons in FTDP-17-1-I/II cultures (Figures 3L and 3M) and significantly increased numbers of $AT8^+/MAP\text{-}2^+$ neurons in FTDP-17-1-I/II and also FTDP-17-2-I/II cultures (Figures 3N and 3O). These findings are consistent with widespread expression of $AT8^+$ p-TAU within the brains of FTDP-17 patients and mutation-specific deposition of $AT8^+$ p-TAU in midbrain DA neurons of patients (Slowinski et al., 2007). In both Ctrl and FTDP-17 neurons, p-TAU showed a punctate expression pattern and was mainly localized to the axonal compartment with some additional perinuclear staining. An intracellular aggregation of p-TAU or a pathologic somatodendritic redistribution of p-TAU was not observed in our cells, as similarly seen in a previous study on iPSC-derived neurons carrying the A152T variant of *MAPT* (Fong et al., 2013).

Neurite Extension Is Impaired in FTDP-17 iPSC-Derived Neurons

Next, we wondered whether the pronounced TAU pathology in FTDP-17 neurons influenced microtubule function, as TAU is a microtubule-associated protein. Neurites from FTDP-17 neurons appeared much shorter and at smaller densities than neurites from Ctrl neurons. Thus, a neurite outgrowth assay, quantifying neurite length of $\beta III\text{-}TUBULIN^+$ neurons 24 and 48 hr after plating, was performed to identify any impairment of neurite extension (Figures 4A–4C). Already 24 hr after plating, the length of FTDP-17-1-I/II and FTDP-17-2-I/II neurons was mildly, but significantly, shorter than those of Ctrl neurons (Figure 4B). By 48 hr, Ctrl neurons had almost doubled their neurite extensions, while FTDP-17 neurons presented with similar neurite lengths as seen at 24 hr after plating (Figure 4B). Only FTDP-17-2-I/II neurons showed a mild but significant increase in neurite length between 24 and 48 hr after seeding (Figure 4B). We performed the same analysis on TH^+ DA Ctrl and FTDP-17 neurons, which revealed similar results (Figure 4C). These observations indicated impaired neurite morphology and complexity in FTDP-17-iPSC-derived neurons.

Increased Oxidative Stress and Activation of the Unfolded Protein Response in FTDP-17 Neurons

FTDP-17 patients show pronounced and widespread neurodegeneration as a result of increased cellular vulnerability. Thus, we next investigated whether FTDP-17 neurons are more susceptible to oxidative stress. We measured responses of Ctrl and FTDP-17 neurons to rotenone, which induces oxidative stress by inhibiting complex I of the mitochondrial respiratory chain (Figures 4D–4G). This experiment revealed increased vulnerability of FTDP-17 neurons toward respiratory stress, as measured by enhanced lactate dehydrogenase (LDH) release 48 hr after application of either 100 or 200 nM rotenone (Figure 4D). Concomitantly, an increased number of $cleaved\text{-}CASPASE\text{-}3^+$ neurons was detected in cultures of FTDP-17 neurons (Figure 4E). Notably, cell death in stressed FTDP-17 neurons significantly declined after application of the antioxidant coenzyme Q10 (0.5 and 1 μM) or the GSK-3 inhibitor CHIR99021 (0.5 and 1 μM; Figures 4F and 4G). These findings indicated that FTDP-17 neurons are more susceptible to oxidative stress and that reversal of oxidative stress is possible in FTDP-17 neurons.

In a variety of neurodegenerative diseases, misfolded proteins accumulate within the ER and activate an ER stress response, which eventually results in apoptosis (Schröder and Kaufman, 2005). Thus, we further investigated whether ER stress is involved in the pathogenesis of FTDP-17. ER stress response is known as the unfolded protein response (UPR) and involves an altered expression of the molecular chaperone binding immunoglobulin protein (BiP), which binds to the protein kinase RNA-like ER kinase (PERK) under unstressed conditions. Upon initiation of ER stress, BiP dissociates from PERK, leading to increased levels of activated phosphorylated PERK (p-PERK) with increased expression of pro-apoptotic proteins such as p53-upregulated modulator of apoptosis (PUMA; Tan et al., 2014). To investigate UPR activation in FTDP-17, we determined expression levels of BiP, p-PERK, and PUMA in FTDP-17 and Ctrl neurons by western blot analysis (Figures 4H and 4I). We found significantly increased levels of BiP, p-PERK, and PUMA in FTDP-17 neurons when compared with Ctrl neurons (Figures 4H and 4I). These findings indicated significant UPR activation in FTDP-17 neurons and pointed toward increased ER stress in FTDP-17.

Altered Gene Expression Profiles in FDTP-17 iPSC-Derived Neurons

We next performed whole-genome transcriptome analysis by microarrays on Ctrl- and FTDP-17 neurons to investigate whether gene expression profiles were altered in FTDP-17 neurons (Figure 5). As expected, expression profiles of both Ctrl- and FTDP-17 neurons differed significantly from undifferentiated iPSCs and formed a separate cluster in the hierarchical cluster analysis reflecting efficient neuronal maturation (Figures 5A and 5B). We investigated genes that were significantly upregulated or downregulated in FTDP-17-1 and FTDP-17-2 neurons in comparison to Ctrl cells (p values ≤ 0.01; Figures 5C–5F, S3A, and S3B; Table S1). This analysis revealed similar, overlapping gene expression profiles in FTDP-17-1 and FTDP-17-2 neurons with 59 upregulated genes in FTDP-17-1 and 42 upregulated genes in FTDP-17-2 neurons (Figure 5C).

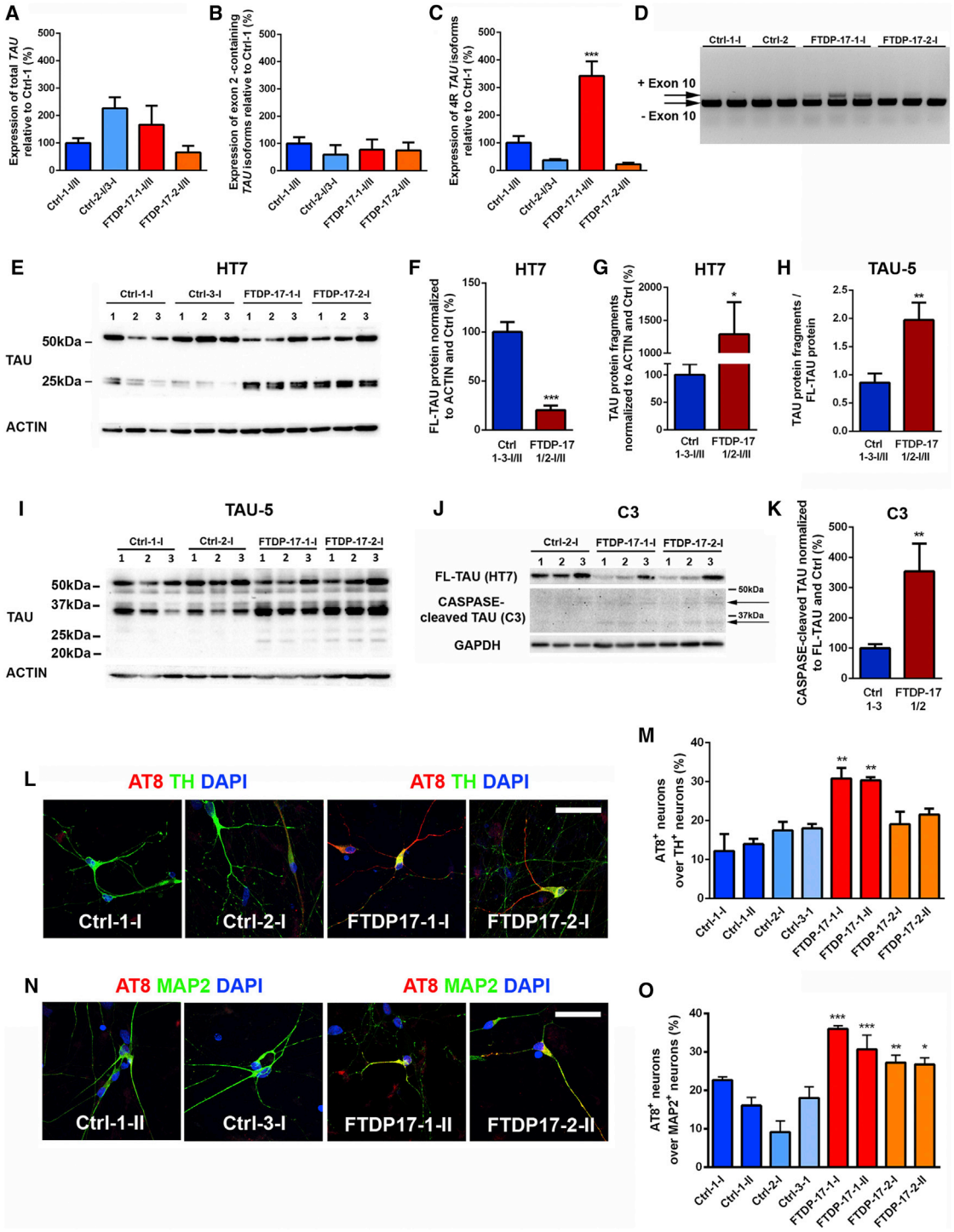

Figure 3. TAU Pathology in FTDP-17 iPSC-Derived Neurons

(A–C) qRT-PCR on Ctrl and FTDP-17 iPSC-derived neurons for (A) total *TAU*, for (B) *TAU* isoforms containing exon 2, and for (C) 4R *TAU* isoforms containing exon 10. Expression levels were normalized to Ctrl-1-I/II and *GAPDH* as housekeeping gene. Data are represented as mean of replicates from three independent experiments per indicated lines (n = 6) +SEM. One-way-ANOVA with post hoc Tukey test was performed for statistical analysis (***p < 0.001).

(D) Electrophoretic separation of 3R and 4R *TAU* isoforms.

(legend continued on next page)

Similarly, compared with Ctrl neurons, 130 and 113 genes were downregulated in FTDP-17-1 and FTDP-17-2 neurons, respectively (Figure 5D). Functional annotation of these downregulated genes was associated with Gene Ontology (GO) terms such as altered monooxygenase activity (*CYP46A1*, *TH*), altered GTPase regulator activity (*ARHGDIB*, *BCR*, *THY1*, *RAPGEF4*), and disturbed cytoskeleton organization and biogenesis (*ADRA2A*, *AMOT*, *ARHGDIB*, *THY1*, *RND1*; Table S1). Downregulated genes also included *PAK3*, a kinase associated with cytoskeletal reorganization and mental retardation (Allen et al., 1998), and *RIT2*, a RAS family GTPase and a susceptibility factor for PD with decreased expression in the SN of patients (Pankratz et al., 2012). Furthermore, we observed significantly decreased expression of *SERP2* (stress-associated ER protein family member 2) and *VGF*, which have been linked to ER and ER-associated stress (Figure 5E; Shimazawa et al., 2010). Functional annotation of upregulated genes was related to GO terms such as cell-cycle arrest (*INHA*) and cellular biosynthesis process (*AK5*, *APOA1*, *INHA*, *RPSY4Y1*, *DMD*; Table S1). Interestingly, particularly highly expressed genes in FTDP-17 neurons included *LOC100128252* (*ZNF667-AS1*), a non-coding RNA transcript with currently unknown function, and *MAGEH1*, an intracellular protein, which interacts with the p75 receptor, a neurotrophin receptor with context-dependent functions promoting either cellular integrity or cellular death to neural cells (Figure 5F; Casaccia-Bonnefil et al., 1999; Tcherpakov et al., 2002).

To investigate a potential role of MAGEH1 in the pathogenesis of FTDP-17, we examined the effects of a *MAGEH1* gene knockdown in FTDP-17 neurons using a lentiviral shRNA expression system. We achieved *MAGEH1* knockdown efficiencies of up to 80% compared with scrambled (scr)-shRNA-expressing FTDP-17 neurons (Figure 5G). We observed an increased susceptibility of FTDP-17 neurons with *MAGEH1* knockdown (FTDP-17-1/2-I/II$^{MAGEH1\text{-}KD}$) to rotenone-induced oxidative stress, as evidenced by an increased number of cleaved-CASPASE-3 and βIII-TUBULIN double$^+$ neurons compared with cultures of scr-shRNA expressing FTDP-17-1/2 neurons (FTDP-17-1/2-I/II^{scr}; Figure 5H). Concomitantly, FTDP-17-1/2-I/II$^{MAGEH1\text{-}KD}$ neurons showed reduced neurite outgrowth compared with FTDP-17-1/2-I/II^{scr} neurons supporting a protective effect of MAGEH1 in FTDP-17 neurons (Figures 5I and 5J). We also found that knockdown of *MAGEH1* in FTDP-17-1/2 neurons was followed by reduced expression of *RIT2* and *PAK3*, which were already downregulated in FTDP-17-1/2 neurons compared with healthy Ctrl cells before the lentiviral treatment (Figures 5E and 5K).

To further elucidate the role of MAGEH1 in differentiated neurons, we overexpressed *MAGEH1* in healthy control cells derived from Ctrl-1/2/3 iPSCs (Figures S3C–S3E). While we did not find any changes in neurite outgrowth after *MAGEH1* overexpression, we observed a significant decrease in the number of cleaved-CASPASE-3$^+$ neurons in rotenone-treated *MAGEH1* overexpressing Ctrl cultures (Ctrl-1/2/3-I/II^{MAGEH1}) when compared with rotenone-treated healthy Ctrl cultures expressing red fluorescent protein (RFP; Ctrl-1/2/3-I/II^{RFP}). These data further supported a putative neuroprotective effect of MAGEH1 in mature neurons.

Some Pathological Changes Are Observed in the Brains of FTDP-17 Patients

Next, we investigated whether pathological changes in FTDP-17 iPSC-derived neurons were also observed in post-mortem brain tissue of FTDP-17 patients (Figures 6A–6H). We collected midbrain tissue from four patients carrying either the N279K mutation or the P301L mutation, another frequent, FTDP-17-causing mutation located in exon 10 of *MAPT*. Consistent with our findings in vitro, we found marked expression of AT8$^+$ p-TAU in DA neurons of the SN and also in non-DA neurons in surrounding brain stem nuclei (Figures 6A and 6B). In contrast to FTDP-17 neurons in vitro, AT8$^+$ p-TAU was deposited as cytoplasmic,

(E–I) Representative western blot analysis on Ctrl and FTDP-17 neurons for TAU protein using the HT7 (E–G) and TAU-5 (H and I) antibodies with the β-ACTIN antibody as loading control. Independent replicates are shown for each line. Quantification of full-length TAU (F) and TAU protein fragments (G) in Ctrl and FTDP-17 neurons using the HT7 antibody. Analysis of TAU-5 western blots showing quantification of ratios of TAU-fragments to full-length TAU (H) in Ctrl and FTDP-17 neurons.

(J and K) Representative western blot on CASPASE-cleaved TAU (J) and quantification of CASPASE-cleaved TAU normalized to full-length TAU (K) in Ctrl and FTDP-17 neurons.

(F–K) Blot quantifications are represented as mean of replicates from three independent differentiation experiments per indicated lines (n = 12 in F–H; n = 9 in K) +SEM. Student's t test was performed for statistical analysis (*p < 0.05, **p < 0.01, ***p < 0.001).

(L and M) Immunostainings of neurons for AT8 (red), TH (green), and DAPI (blue) (L) with quantification (M).

(N and O) Immunostainings of neurons for AT8 (red), MAP2 (green), and DAPI (blue) (N) with quantification (O).

(L–O) Data in (M) and (O) are represented as means of replicates from three independent differentiation experiments +SEM. One-way-ANOVA with post hoc Tukey test was performed for statistical analysis (*p < 0.05, **p < 0.01, ***p < 0.001). Scale bars in (L) and (N) represent 50 μm.

See also Figure S2.

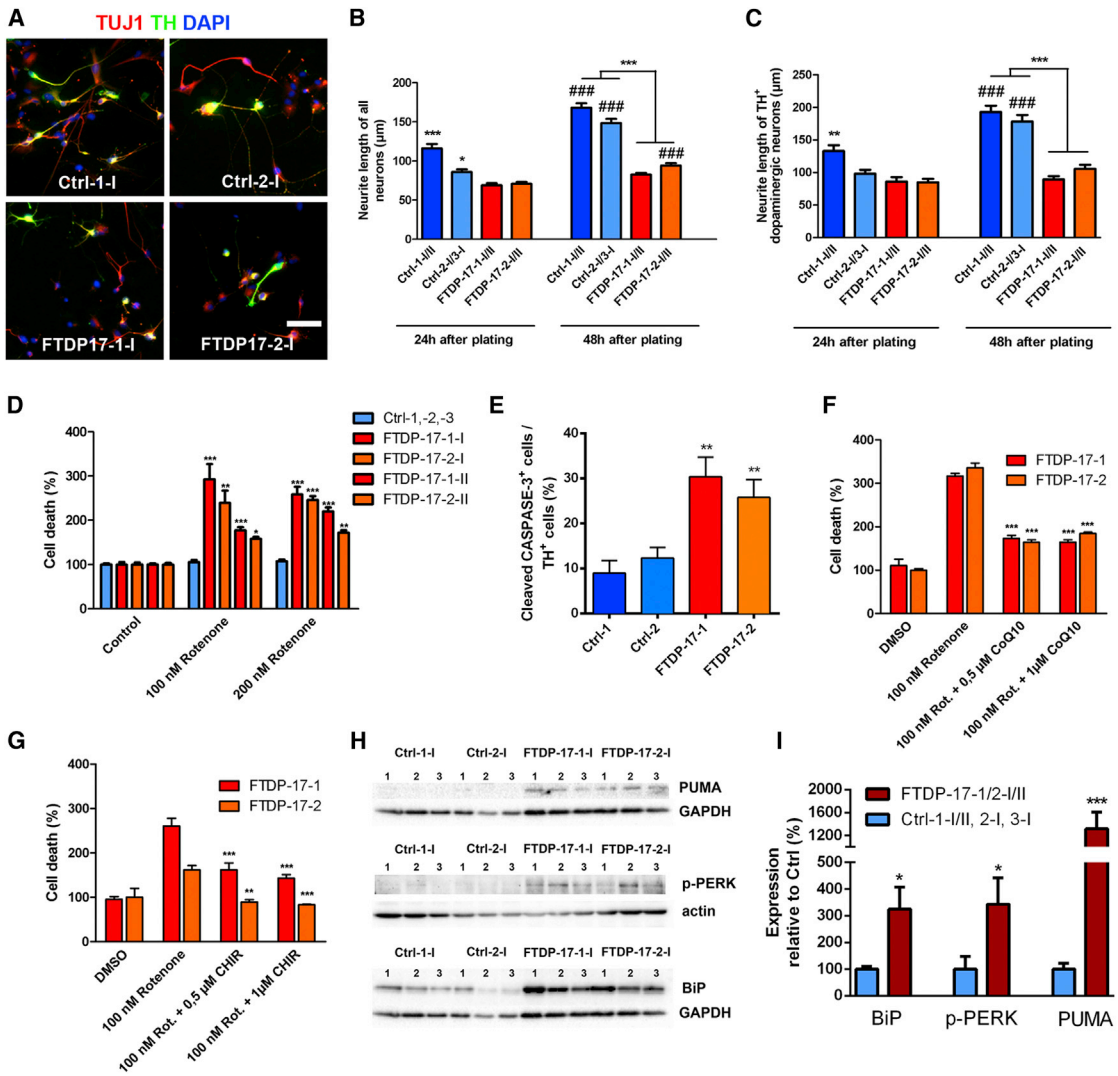

Figure 4. Decreased Neurite Outgrowth, Enhanced Vulnerability to Oxidative Stress, and Activation of the UPR in FTDP-17 Neurons

(A) Immunostainings of Ctrl and FTDP-17 neurons for TH (green) and TUJ1 (red) 48 hr after plating. Nuclei were stained with DAPI.

(B and C) Quantification of neurite outgrowth in (B) βIII-TUBULIN$^+$ neurons and in (C) TH$^+$ DA neurons 24 hr and 48 hr after plating. Neurite outgrowth was assessed by measurement of the longest neurite of each neuron. Data are represented as mean of at least 100 measurements per indicated lines from three independent experiments +SEM. Two-way ANOVA with post hoc Tukey test was used as statistical test (*$p < 0.05$, **$p < 0.01$, ***$p < 0.001$; $^{###}p < 0.001$: denotes effect over time within groups).

(D) Effect of oxidative stress on FTDP-17 and Ctrl neurons analyzed by measurement of LDH release after 48 hr of rotenone treatment.

(E) Quantification of cleaved-CASPASE-3$^+$ DA neurons in Ctrl and FTDP-17 cultures after 48 hr of rotenone treatment.

(F and G) Rescue of FTDP-17 neurons through treatment with (F) CoQ10 or (G) the GSK-3 inhibitor CHIR99021.

(D–G) Data are represented as mean of replicates from three independent experiments +SEM. One-way ANOVA with post hoc Tukey test was used as statistical test (*$p < 0.05$, **$p < 0.01$, ***$p < 0.001$).

(H) Western blot analyses of ER stress-associated markers PUMA, p-PERK, and BiP in Ctrl and FTDP-17 neurons. GAPDH or β-ACTIN was used as a loading control.

(I) Quantifications of protein expression in FTDP-17 neurons relative to expression in Ctrl neurons and to expression of GAPDH or β-ACTIN, respectively. Data are represented as mean of replicates from three independent differentiation experiments per indicated lines ($n = 12$) +SEM. Student's t test was used as statistical test (*$p < 0.05$; ***$p < 0.001$).

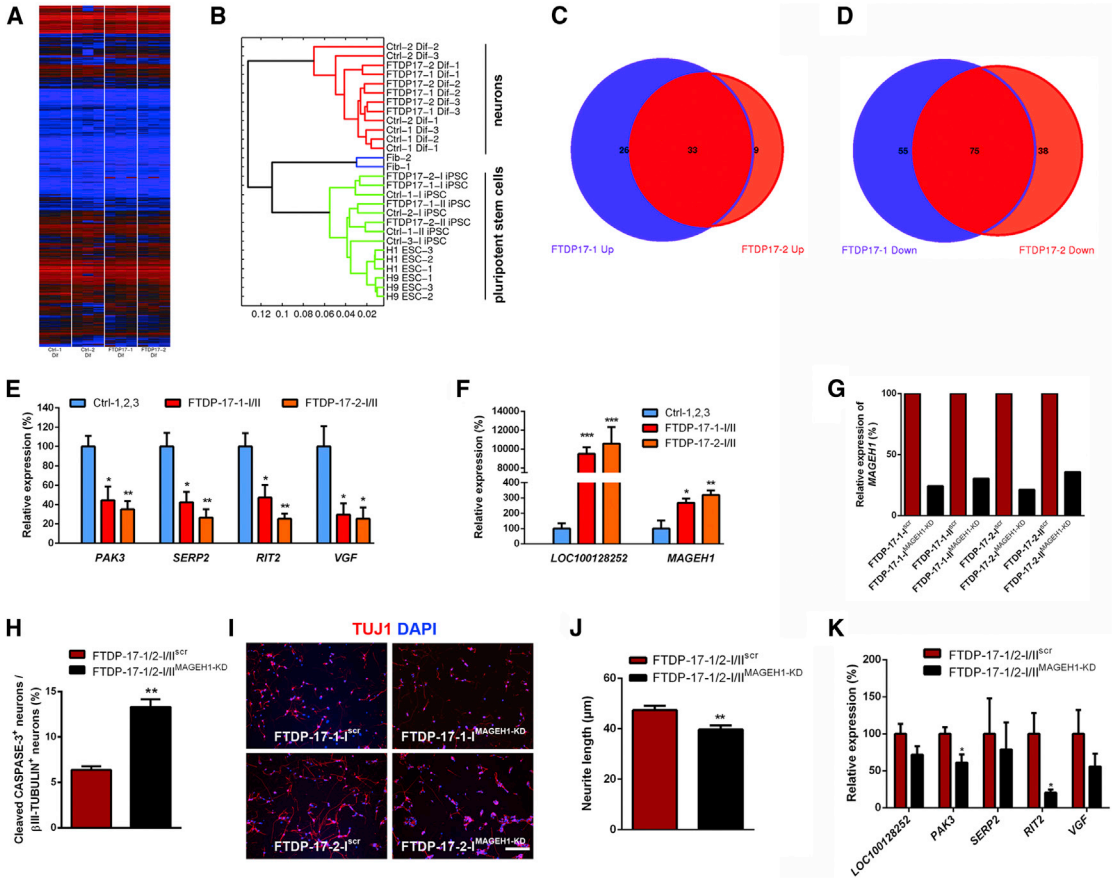

Figure 5. Gene Expression Profiles in FTDP-17 and Ctrl Neurons

Whole-genome transcriptome microarray analysis of Ctrl and FTDP-17 neurons derived from three independent differentiations.

(A and B) Whole genome expression profiles presented as (A) heatmap and (B) hierarchical clustering dendrogram.

(C and D) Venn diagram showing the overlap of genes significantly upregulated (C) or downregulated (D) in FTDP-17-1 and FTDP-17-2 neurons.

(E and F) Validation of differentially downregulated (E) and upregulated (F) genes by qRT-PCR. Data are represented as mean of replicates from three independent experiments per indicated lines +SEM. One-way ANOVA with post hoc Tukey test was used as statistical test (*$p < 0.05$, **$p < 0.01$, ***$p < 0.001$).

(G) Relative gene expression of *MAGEH1* in FTDP-17-1/2-I/II$^{MAGEH1\text{-}KD}$ or FTDP-17-1/2-I/II^{scr} control neurons.

(H) Quantification of cleaved-CASPASE-3^{+} neurons in FTDP-17-1/2-I/II$^{MAGEH1\text{-}KD}$ or FTDP-17-1/2-I/II^{scr} control neurons after 48 hr of rotenone treatment. At least 800 cells were counted per cell line and differentiation.

(I) Immunostainings of FTDP-17-1/2-I/II$^{MAGEH1\text{-}KD}$ or FTDP-17-1/2-I/II^{scr} control neurons for βIII-TUBULIN 48 hr after plating as single cells. Nuclei were stained with DAPI.

(J) Quantification of neurite outgrowth in cultures of FTDP-17-1/2-I/II$^{MAGEH1\text{-}KD}$ or FTDP-17-1/2-I/II^{scr} control neurons 48 hr after plating. At least 100 neurons were measured per cell line and differentiation.

(K) Relative expression of the indicated genes in FTDP-17-1/2-I/II$^{MAGEH1\text{-}KD}$ or FTDP-17-1/2-I/II^{scr} control neurons.

(H, J, and K) Data are presented as mean of independent replicates from four different lines +SEM. Student's t test was performed for statistical analysis (*$p < 0.05$, **$p < 0.01$).

See also Figure S3 and Table S1.

perinuclear aggregates within neurons and as neurofibrillary tangles (NFTs) within axonal projections, which appeared morphologically disturbed (Figures 6A and 6B). AT8^{+} deposits were also identified in glial cells (Figure 6A). An analysis of AT8 distribution within the temporal cortex of FTDP-17 patients revealed similar results (Figure 6A). These changes were accompanied by significant neuronal cell loss.

The expression of 4R *TAU* was increased in the patient's brains (Figure 6C), and in line with our in vitro

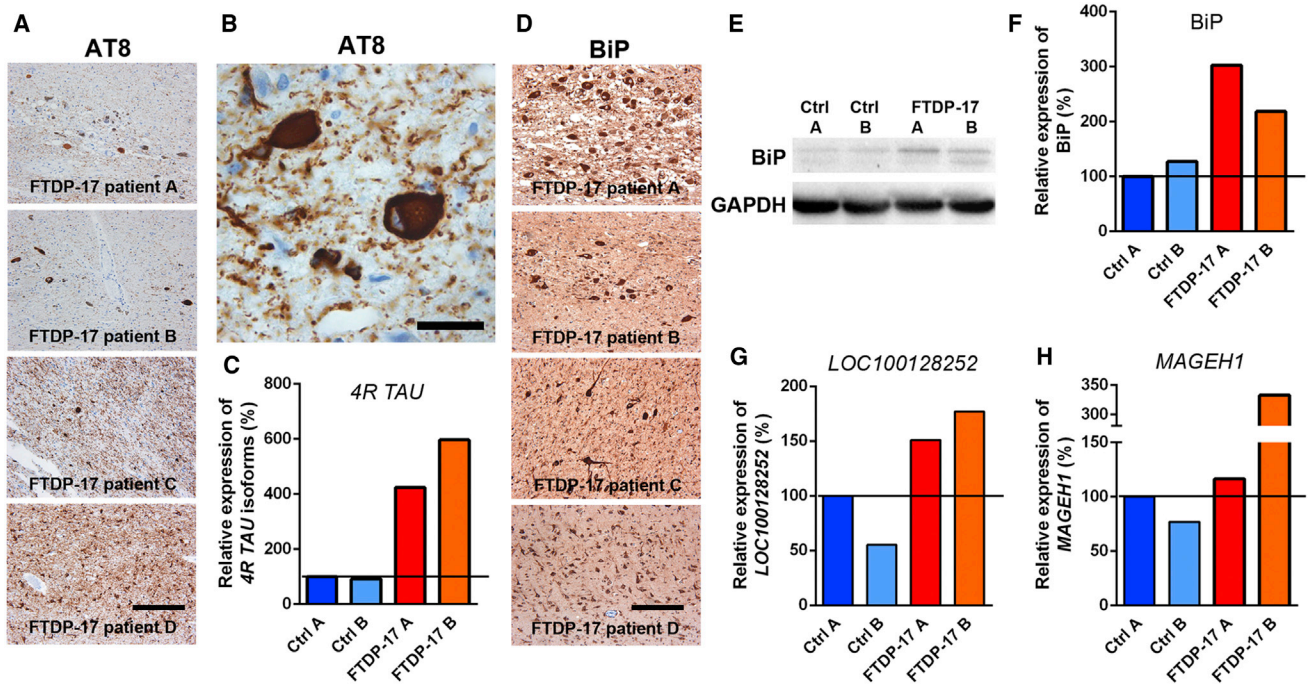

Figure 6. Identification of Pathological Changes in Post-mortem Tissue from FTDP-17 Patients

(A and B) Immunostaining for AT8 demonstrating pronounced p-TAU expression in neurons and glial cells in the midbrain (patients A–C) and temporal cortex (patient D) of FTDP-17 patients carrying the P301L *MAPT* mutation (patients A and B) or the N279K *MAPT* mutation (patients C and D). The scale bar represents 200 μm. Higher magnification image in (B) reveals AT8 immunoreactivity in FTDP-17 midbrain neurons with neuropil threads. The scale bar represents 20 μm.

(C) qRT-PCR for detection of 4R *TAU* isoforms in Ctrl individual and FTDP-17 patient midbrain samples.

(D) Immunostaining for the ER stress marker BiP in the midbrain (patients A–C) and temporal cortex (patient D) of FTDP-17 patients. The scale bar represents 200 μm.

(E) Western blot analysis of BiP expression in the midbrain of Ctrl individuals and FTDP-17 patients. GAPDH expression was used as loading control.

(F) Quantification of BiP expression in FTDP-17 patients relative to Ctrl A and normalized to GAPDH expression.

(G and H) qRT-PCR for detection of (G) *LOC100128252* and (H) *MAGEH1* in Ctrl individual and FTDP-17 patient midbrain samples.

(C, G, and H) Data were normalized to *GAPDH* expression and to Ctrl A and are represented as mean of triplicates from the same tissue preparation.

observations of increased UPR activation in FTDP-17 neurons, we found abundant expression of BiP protein within DA and non-DA neurons in histological specimen from all four FTDP-17 patients (Figure 6D). Since BiP is expressed to certain extents also under normal conditions, we quantified expression levels by western blot analysis and processed native, fresh-frozen midbrain tissue from two FTDP-17 patients and from two Ctrl individuals for molecular analyses. We observed increased levels of BiP protein in samples from FTDP-17 patients as similarly seen in in vitro-differentiated FTDP-17 iPSCs (Figures 6E and 6F).

Likewise, we found that some of the aforementioned dysregulated genes in FTDP-17 iPSC-derived neurons were also dysregulated in post-mortem tissue from FTDP-17 patients. Indeed, while *PAK3*, *RIT2*, *SERP2*, and *VGF* were not downregulated in post-mortem tissue of FTDP-17 patients, we observed that *LOC100128252* and *MAGEH1*, which were particularly strongly expressed in FTDP-17 neurons, were also more strongly expressed in post-mortem tissue of FTDP-17 patients compared with Ctrl individuals (Figures 6G and 6H). These data further indicated that these two molecules with currently unknown function in the context of neurodegeneration could play a significant role during FTDP-17 pathogenesis.

DISCUSSION

We used iPSC-derived neurons to identify distinct neurodegenerative changes in FTDP-17. We found that overall neuronal differentiation was not impaired in FTDP-17 iPSCs. However, FTDP-17 neurons presented

with disturbed neurite morphology as well as with impaired neurite extension and exhibited distinct TAU pathology with increased fragmentation of full-length TAU protein and an increased immunoreactivity for AT8. FTDP-17 neurons displayed increased and reversible vulnerability toward oxidative stress and presented with activated UPR. Furthermore, we have identified genes, which were significantly dysregulated in FTDP-17 neurons, including an upregulation of *LOC100128252* and *MAGEH1*. Notably, some of these pathologic changes could also be identified in post-mortem material from patients with FTDP-17.

FTDP-17 is caused by *MAPT* mutations, which lead to either increased expression of 4R TAU isoforms or to decreased interaction of TAU protein with microtubules (Goedert and Spillantini, 2011). As such, we reasoned to examine FTDP-17 iPSCs, which have been derived from individuals carrying *MAPT* mutations representing the former and the latter group, respectively. Only FTDP-17-1 neurons carrying the N279K mutation expressed increased amounts of 4R *TAU* transcripts, while FTDP-17-2 neurons carrying the V337M mutation showed normal 4R *TAU* expression levels, thus reflecting observations made in vivo. Despite these differences in 4R *TAU* expression, most of the observed FTDP-17 disease phenotypes were almost identical and appeared to similar extents in FTDP-17-1 and FTDP-17-2 neurons. The major mutation-specific difference comprised an increased expression of $AT8^+$ p-TAU in FTDP-17-1 neurons, but not in FTDP-17-2 DA neurons. In contrast, non-DA neurons from both FTDP-17 patients presented with significantly increased AT8 positivity as compared with the Ctrl groups. These findings are in line with observations made in vivo, as deposition of $AT8^+$ p-TAU is especially observed in SN DA neurons of patients carrying the N279K mutation. On the other hand, excessive and widespread AT8 positivity is found in non-DA neurons in brains of patients with the N279K mutation and in patients with the V337M mutation. Thus, findings in vivo were mimicked in vitro validating our iPSC-based model of FTDP-17.

Both the N279K and the V337M mutation render the TAU protein more susceptible to hyperphosphorylation (Alonso Adel et al., 2004). When tau becomes hyperphosphorylated, it detaches from microtubules and destabilizes microtubule assemblies, thereby affecting microtubule function (Noble et al., 2013). These findings could explain the impairment of neurite outgrowth in FTDP-17 neurons. Furthermore, we found an increased fragmentation of TAU protein in FTDP-17 neurons at the expense of full-length TAU, which most likely further contributed to disturbed neurite morphology. Increased TAU fragmentation and abnormal neurite morphologies were previously described in iPSC-derived neurons carrying the A152T variant of *MAPT*, which may increase the risk for the development of FTD, PSP, and AD (Fong et al., 2013). In this study, heterozygous A152T neurons showed a similar increase in TAU fragmentation as compared with gene-corrected control cells. This effect could further be potentiated by the introduction of a second mutation at the same site. Thus, these data support our observation that genetic changes in *MAPT* can have significant effects on the structural integrity of TAU. Fragmentation of TAU can occur through cleavage by several caspases including caspase-3 (Fasulo et al., 2000). We observed that increased TAU fragmentation in FTDP-17 neurons was at least in part mediated by CASPASE-driven proteolysis, as evidenced by the detection of a truncated TAU protein, which is recognized at its C terminus by a CASPASE-cleaved TAU-specific antibody. This CASPASE-associated fragmentation was not specific to the N279K and V337M mutation but also occurred to a similar extent in neurons carrying the A152T *MAPT* variant (Fong et al., 2013). Interestingly, however, our N279K and V337M mutant FTDP-17 neurons expressed an additional low-molecular-weight variant of CASPASE-cleaved TAU, indicating that a fraction of CASPASE-cleaved TAU was further truncated at its N terminus by additional proteases. These data encourage performing additional comparative studies on iPSC-derived neurons from patients with different *MAPT* mutations to better characterize mutation-specific expression profiles of proteases in FTDP-17.

TAU fragments carry an apoptosis-inducing activity, which is further potentiated when cells are exposed to TAU fragments carrying the N279K mutation (Fasulo et al., 2005). In addition, overexpression of full-length TAU carrying the N279K or the V337M mutation resulted in induction of apoptosis after serum deprivation (Furukawa et al., 2000). These findings are consistent with our data demonstrating an increased vulnerability of FTDP-17 neurons toward oxidative stress induced by the mitochondrial complex I inhibitor rotenone. This response was accompanied by an increased expression of cleaved-CASPASE-3. Rotenone-induced cytotoxicity has been observed in an iPSC-based model of PD (Reinhardt et al., 2013b), which is characterized by an increased vulnerability of midbrain DA neurons as similarly seen in FTDP-17. Increased cell death of FTDP-17 neurons could, at least in part and in addition to increased TAU fragmentation, be related to a direct impact of the N279K and V337M mutations on mitochondrial function. Such an effect was recently described for P301L mutant TAU, which when overexpressed in a neuroblastoma cell line led to reduced mitochondrial complex I activity and to an increased vulnerability toward H_2O_2-mediated oxidative stress (Schulz et al., 2012).

Stress responses were reversible, as the antioxidant coenzyme Q10 prevented cell death in challenged FTDP-17

neurons. Furthermore, GSK-3 inhibition in FTDP-17 neurons by CHIR99021 resulted in overall rescue of cell viability, consistent with a pro-apoptotic function of GSK-3 in the context of oxidative stress, as shown in SH-SY5Y cells (King and Jope, 2005). Furthermore, GSK-3-β showed increased activity in SH-SY5Y cells upon UPR activation (Song et al., 2002), which was readily observed in our FTDP-17 iPSC-derived neurons. These experiments provided proof of principle that an intervention is possible to prevent cell death in patients' neurons at risk. At the same time, they highlight the unique potential of iPSCs to identify potentially beneficial compounds in FTDP-17, as human neurons can be produced efficiently and at high numbers for high-throughput drug screening purposes (Heilker et al., 2014).

While UPR is initially a protective response mechanism toward misfolded proteins, its prolonged activation can lead to the onset of apoptosis and eventually to cell death. We observed an upregulation of BiP protein in FTDP-17 neurons, which was accompanied by an increased expression of p-PERK and the apoptosis-inducing protein PUMA. These findings indicated increased ER stress as a contributing factor to FTDP-17. In line with this observation, we also found UPR activation in the brains of patients with FTDP-17. UPR activation has been described in brains of patients with AD and in cases of FTDL-TAU (Hoozemans et al., 2009; Nijholt et al., 2012). In neurons of AD patients, markers of UPR activation appeared at early stages of disease development and were co-expressed with AT8 prior to NFT formation (Hoozemans et al., 2009). Furthermore, a recent whole-genome association study for PSP identified a small nuclear polymorphism in *EIF2AK3*, the gene encoding PERK, as a risk factor for the development of PSP (Höglinger et al., 2011). These studies and our present data on FTDP-17 neurons thus demonstrate that TAU pathology is closely linked to ER stress in tauopathies. The mechanisms, however, by which TAU interferes with ER function and UPR are still unclear, as TAU is located in the cytoplasm and not in the ER (Abisambra et al., 2013).

Our whole-genome expression analysis identified dysregulated genes in FTDP-17 neurons. Downregulated genes included *PAK3* and *RIT2*, which have been linked to mental retardation (Allen et al., 1998) and PD (Pankratz et al., 2012), respectively. Upregulated genes included *LOC100128252 (ZNF667-AS1)*, a non-coding RNA transcript with currently unknown function, and the intracellular molecule *MAGEH1*, both of which were also highly expressed in the post-mortem brains of FTDP-17 patients. While further studies have to be performed to characterize the function of LOC100128252 in the context of FTDP-17, we could identify a beneficial role of MAGEH1 in patient-derived neurons. Our *MAGEH1* knockdown experiments revealed increased susceptibility of FTDP-17 neurons to oxidative stress and demonstrated reduced neurite outgrowth. Accordingly, overexpression of *MAGEH1* in healthy control neurons resulted in reduced vulnerability toward oxidative stress, suggesting that upregulation of MAGEH1 in FTDP-17 neurons represents a so far unknown endogenous neuroprotective mechanism. MAGEH1 can associate with the intracellular domain of the p75 receptor (Tcherpakov et al., 2002), which has been linked to cell survival and differentiation in neural progenitor cells (Casaccia-Bonnefil et al., 1999). It remains to be shown whether the beneficial effects of MAGEH1 in FTDP-17 neurons involve the p75 receptor and further studies are necessary to identify the mechanisms by which MAGEH1 promotes neuroprotection in FTDP-17 neurons.

In conclusion, our iPSC-based model of FTDP-17 is well suited for identifying pathways involved in neurodegenerative processes in FTDP-17 as it captures a large variety of disease-specific phenotypes and offers the possibility to analyze disease-affected cells in vitro. At the same time, it provides the unique opportunity to use these cells as a platform for drug screening purposes to establish therapeutic approaches in FTDP-17.

EXPERIMENTAL PROCEDURES

Derivation of iPSCs

Fibroblasts from individuals with *MAPT* mutations, here referred to as FTDP-17 patients, were obtained from the Coriell Institute for Medical Research and were reprogrammed using a lentiviral SF-OSKM-tomato expression vector. See the Supplemental Experimental Procedures for further details, which also includes a list of antibodies used in this study (Table S2) and a list of the primers employed for qRT-PCR analyses (Table S3). The work with human ESCs has been approved by the Robert Koch Institute (Az. 1710-79-1-4-55-E1).

Neurite Outgrowth Assays

After 22 days of terminal differentiation, neurons were singularized by treatment with accutase (PAA) for approximately 10 min at 37°C. Cells were subsequently diluted in DMEM (PAA) and spun down at 200 × *g* for 5 min. The cell pellet was resuspended in neuronal maturation medium, and cells were plated on matrigel-coated 48-well plates at a density of 3×10^4 cells per well. At 24 and 48 hr after plating, cells were fixed in 4% paraformaldehyde (Electron Microscopy Sciences) for 20 min at 4°C, and neurons were stained for βIII-TUBULIN and TH. Neurite outgrowth was analyzed in a double-blinded manner on random fluorescence images and on at least 100 neurons per iPSC clone using the Image J software.

Stress-Induced Cell Death and Rescue

Neurons were replated after 10 days of neuronal differentiation at a density of 8×10^3 cells per well into 96-well plates. After another 11 days in maturation medium, 100 and 200 nM rotenone (Sigma) in N2 medium consisting of DMEM-F12 with 1:100 N2 supplement and 1% penicillin/streptomycin/glutamine were added to

the cells for 24 hr. Viability was assessed by measuring LDH leakage in the supernatant using the Cytotoxicity Detection Kit Plus (Roche). Absorbance was recorded at 490 nm and was expressed as the percentage of absorbance in control cells after subtraction of background absorbance. For rescue experiments, 0.5 and 1 μM CHIR99021 (Axon Medchem) was added to the medium 48 hr before and throughout rotenone treatment, and 0.5 and 1 μM Coenzyme Q10 (Sigma) was added to the medium 20 min before measurement.

Statistics

Data of at least three independent differentiation experiments are presented as mean + SEM. Statistical significance was determined by Student's t test and with one-way ANOVA and two-way ANOVA with post hoc Tukey test, respectively.

ACCESSION NUMBERS

The accession number for the data discussed in this publication is GEO: GSE62935 (http://www.ncbi.nlm.nih.gov/geo/query/acc.cgi$acc=GSE62935).

SUPPLEMENTAL INFORMATION

Supplemental Information includes Supplemental Experimental Procedures, three figures, and three tables and can be found with this article online at http://dx.doi.org/10.1016/j.stemcr.2015.06.001.

AUTHOR CONTRIBUTIONS

M.E., A.-L.H., H.R.S., J.S., T.K., and G.H. developed and designed the study. M.E., A.-L.H., P.R., S.K., A.R., O.E.P., A.L.O., J.R.M., B.G., H.Z., and G.H. performed experiments. M.E., A.-L.H., P.R., M.J.A.-B., S.K., A.R., M.G., P.E., S.G.M., B.G., A.R., H.Z., J.S., T.K., and G.H. analyzed data. M.E., A.-L.H., J.S., T.K., and G.H. wrote the manuscript. P.R. and M.J.-A.-B. contributed equally.

ACKNOWLEDGMENTS

We thank Martina Radstaak, Ingrid Gelker, Elke Hoffmann, Claudia Kemming, Claudia Ortmeier, Martina Sinn, and Susanne Peetz-Dienhart for outstanding technical assistance and Axel Schambach and Christopher Baum, MHH, Hannover, Germany, for providing the lentiviral SFFV reprogramming vector. This study was supported by research funding from the IMF at University Hospital Münster to G.H. and P.E. (I-HA-111219 and AL121108), from the U.S. Public Health Service to B.G. (P30 AG10133), from the German Research Foundation (DFG) to J.S. and P.R. (STE 1835/1-1, GA 402/18-1, FZT 111 DFG, Center for Regenerative Therapies Dresden, Cluster of Excellence), from the DFG to T.K. (SFB-TRR128-B7), and from the German Federal Ministry of Education and Research to H.R.S. and H.Z. (BMBF 01GN0811 and 01GN1008B).

Received: November 16, 2014
Revised: June 8, 2015
Accepted: June 8, 2015
Published: July 2, 2015

REFERENCES

Abisambra, J.F., Jinwal, U.K., Blair, L.J., O'Leary, J.C., 3rd, Li, Q., Brady, S., Wang, L., Guidi, C.E., Zhang, B., Nordhues, B.A., et al. (2013). Tau accumulation activates the unfolded protein response by impairing endoplasmic reticulum-associated degradation. J. Neurosci. *33*, 9498–9507.

Allen, K.M., Gleeson, J.G., Bagrodia, S., Partington, M.W., MacMillan, J.C., Cerione, R.A., Mulley, J.C., and Walsh, C.A. (1998). PAK3 mutation in nonsyndromic X-linked mental retardation. Nat. Genet. *20*, 25–30.

Almeida, S., Zhang, Z., Coppola, G., Mao, W., Futai, K., Karydas, A., Geschwind, M.D., Tartaglia, M.C., Gao, F., Gianni, D., et al. (2012). Induced pluripotent stem cell models of progranulin-deficient frontotemporal dementia uncover specific reversible neuronal defects. Cell Rep. *2*, 789–798.

Almeida, S., Gascon, E., Tran, H., Chou, H.J., Gendron, T.F., Degroot, S., Tapper, A.R., Sellier, C., Charlet-Berguerand, N., Karydas, A., et al. (2013). Modeling key pathological features of frontotemporal dementia with C9ORF72 repeat expansion in iPSC-derived human neurons. Acta Neuropathol. *126*, 385–399.

Alonso Adel, C., Mederlyova, A., Novak, M., Grundke-Iqbal, I., and Iqbal, K. (2004). Promotion of hyperphosphorylation by frontotemporal dementia tau mutations. J. Biol. Chem. *279*, 34873–34881.

Boxer, A.L., and Miller, B.L. (2005). Clinical features of frontotemporal dementia. Alzheimer Dis. Assoc. Disord. *19* (*Suppl 1*), S3–S6.

Casaccia-Bonnefil, P., Gu, C., Khursigara, G., and Chao, M.V. (1999). p75 neurotrophin receptor as a modulator of survival and death decisions. Microsc. Res. Tech. *45*, 217–224.

Cooper, O., Seo, H., Andrabi, S., Guardia-Laguarta, C., Graziotto, J., Sundberg, M., McLean, J.R., Carrillo-Reid, L., Xie, Z., Osborn, T., et al. (2012). Pharmacological rescue of mitochondrial deficits in iPSC-derived neural cells from patients with familial Parkinson's disease. Sci. Transl. Med. *4*, 141ra190.

Fasulo, L., Ugolini, G., Visintin, M., Bradbury, A., Brancolini, C., Verzillo, V., Novak, M., and Cattaneo, A. (2000). The neuronal microtubule-associated protein tau is a substrate for caspase-3 and an effector of apoptosis. J. Neurochem. *75*, 624–633.

Fasulo, L., Ugolini, G., and Cattaneo, A. (2005). Apoptotic effect of caspase-3 cleaved tau in hippocampal neurons and its potentiation by tau FTDP-mutation N279K. J. Alzheimers Dis. *7*, 3–13.

Fong, H., Wang, C., Knoferle, J., Walker, D., Balestra, M.E., Tong, L.M., Leung, L., Ring, K.L., Seeley, W.W., Karydas, A., et al. (2013). Genetic correction of tauopathy phenotypes in neurons derived from human induced pluripotent stem cells. Stem Cell Reports *1*, 226–234.

Furukawa, K., D'Souza, I., Crudder, C.H., Onodera, H., Itoyama, Y., Poorkaj, P., Bird, T.D., and Schellenberg, G.D. (2000). Pro-apoptotic effects of tau mutations in chromosome 17 frontotemporal dementia and parkinsonism. Neuroreport *11*, 57–60.

Ghetti, B., Oblak, A.L., Boeve, B.F., Johnson, K.A., Dickerson, B.C., and Goedert, M. (2015). Invited review: Frontotemporal dementia caused by microtubule-associated protein tau gene (MAPT) mutations: a chameleon for neuropathology and neuroimaging. Neuropathol. Appl. Neurobiol. *41*, 24–46.

Goedert, M., and Spillantini, M.G. (2011). Pathogenesis of the tauopathies. J. Mol. Neurosci. *45*, 425–431.

Goedert, M., Spillantini, M.G., Jakes, R., Rutherford, D., and Crowther, R.A. (1989). Multiple isoforms of human microtubule-associated protein tau: sequences and localization in neurofibrillary tangles of Alzheimer's disease. Neuron *3*, 519–526.

Goedert, M., Ghetti, B., and Spillantini, M.G. (2012). Frontotemporal dementia: implications for understanding Alzheimer disease. Cold Spring Harb Perspect Med *2*, a006254.

Hargus, G., Cooper, O., Deleidi, M., Levy, A., Lee, K., Marlow, E., Yow, A., Soldner, F., Hockemeyer, D., Hallett, P.J., et al. (2010). Differentiated Parkinson patient-derived induced pluripotent stem cells grow in the adult rodent brain and reduce motor asymmetry in Parkinsonian rats. Proc. Natl. Acad. Sci. USA *107*, 15921–15926.

Hargus, G., Ehrlich, M., Araúzo-Bravo, M.J., Hemmer, K., Hallmann, A.L., Reinhardt, P., Kim, K.P., Adachi, K., Santourlidis, S., Ghanjati, F., et al. (2014a). Origin-dependent neural cell identities in differentiated human iPSCs in vitro and after transplantation into the mouse brain. Cell Rep. *8*, 1697–1703.

Hargus, G., Ehrlich, M., Hallmann, A.L., and Kuhlmann, T. (2014b). Human stem cell models of neurodegeneration: a novel approach to study mechanisms of disease development. Acta Neuropathol. *127*, 151–173.

Heilker, R., Traub, S., Reinhardt, P., Schöler, H.R., and Sterneckert, J. (2014). iPS cell derived neuronal cells for drug discovery. Trends Pharmacol. Sci. *35*, 510–519.

Höglinger, G.U., Melhem, N.M., Dickson, D.W., Sleiman, P.M., Wang, L.S., Klei, L., Rademakers, R., de Silva, R., Litvan, I., Riley, D.E., et al.; PSP Genetics Study Group (2011). Identification of common variants influencing risk of the tauopathy progressive supranuclear palsy. Nat. Genet. *43*, 699–705.

Hoozemans, J.J., van Haastert, E.S., Nijholt, D.A., Rozemuller, A.J., Eikelenboom, P., and Scheper, W. (2009). The unfolded protein response is activated in pretangle neurons in Alzheimer's disease hippocampus. Am. J. Pathol. *174*, 1241–1251.

Iovino, M., Patani, R., Watts, C., Chandran, S., and Spillantini, M.G. (2010). Human stem cell-derived neurons: a system to study human tau function and dysfunction. PLoS ONE *5*, e13947.

Irwin, D.J., Cairns, N.J., Grossman, M., McMillan, C.T., Lee, E.B., Van Deerlin, V.M., Lee, V.M., and Trojanowski, J.Q. (2015). Frontotemporal lobar degeneration: defining phenotypic diversity through personalized medicine. Acta Neuropathol. *129*, 469–491.

King, T.D., and Jope, R.S. (2005). Inhibition of glycogen synthase kinase-3 protects cells from intrinsic but not extrinsic oxidative stress. Neuroreport *16*, 597–601.

Knopman, D.S., and Roberts, R.O. (2011). Estimating the number of persons with frontotemporal lobar degeneration in the US population. J. Mol. Neurosci. *45*, 330–335.

Nijholt, D.A., van Haastert, E.S., Rozemuller, A.J., Scheper, W., and Hoozemans, J.J. (2012). The unfolded protein response is associated with early tau pathology in the hippocampus of tauopathies. J. Pathol. *226*, 693–702.

Noble, W., Hanger, D.P., Miller, C.C., and Lovestone, S. (2013). The importance of tau phosphorylation for neurodegenerative diseases. Front Neurol. *4*, 83.

Pankratz, N., Beecham, G.W., DeStefano, A.L., Dawson, T.M., Doheny, K.F., Factor, S.A., Hamza, T.H., Hung, A.Y., Hyman, B.T., Ivinson, A.J., et al.; PD GWAS Consortium (2012). Meta-analysis of Parkinson's disease: identification of a novel locus, RIT2. Ann. Neurol. *71*, 370–384.

Reinhardt, P., Glatza, M., Hemmer, K., Tsytsyura, Y., Thiel, C.S., Höing, S., Moritz, S., Parga, J.A., Wagner, L., Bruder, J.M., et al. (2013a). Derivation and expansion using only small molecules of human neural progenitors for neurodegenerative disease modeling. PLoS ONE *8*, e59252.

Reinhardt, P., Schmid, B., Burbulla, L.F., Schöndorf, D.C., Wagner, L., Glatza, M., Höing, S., Hargus, G., Heck, S.A., Dhingra, A., et al. (2013b). Genetic correction of a LRRK2 mutation in human iPSCs links parkinsonian neurodegeneration to ERK-dependent changes in gene expression. Cell Stem Cell *12*, 354–367.

Schröder, M., and Kaufman, R.J. (2005). The mammalian unfolded protein response. Annu. Rev. Biochem. *74*, 739–789.

Schulz, K.L., Eckert, A., Rhein, V., Mai, S., Haase, W., Reichert, A.S., Jendrach, M., Müller, W.E., and Leuner, K. (2012). A new link to mitochondrial impairment in tauopathies. Mol. Neurobiol. *46*, 205–216.

Shimazawa, M., Tanaka, H., Ito, Y., Morimoto, N., Tsuruma, K., Kadokura, M., Tamura, S., Inoue, T., Yamada, M., Takahashi, H., et al. (2010). An inducer of VGF protects cells against ER stress-induced cell death and prolongs survival in the mutant SOD1 animal models of familial ALS. PLoS ONE *5*, e15307.

Slowinski, J., Dominik, J., Uitti, R.J., Ahmed, Z., Dickson, D.D., and Wszolek, Z.K. (2007). Frontotemporal dementia and Parkinsonism linked to chromosome 17 with the N279K tau mutation. Neuropathology *27*, 73–80.

Soldner, F., Hockemeyer, D., Beard, C., Gao, Q., Bell, G.W., Cook, E.G., Hargus, G., Blak, A., Cooper, O., Mitalipova, M., et al. (2009). Parkinson's disease patient-derived induced pluripotent stem cells free of viral reprogramming factors. Cell *136*, 964–977.

Song, L., De Sarno, P., and Jope, R.S. (2002). Central role of glycogen synthase kinase-3beta in endoplasmic reticulum stress-induced caspase-3 activation. J. Biol. Chem. *277*, 44701–44708.

Tan, S., Wei, X., Song, M., Tao, J., Yang, Y., Khatoon, S., Liu, H., Jiang, J., and Wu, B. (2014). PUMA mediates ER stress-induced apoptosis in portal hypertensive gastropathy. Cell Death Dis. *5*, e1128.

Tcherpakov, M., Bronfman, F.C., Conticello, S.G., Vaskovsky, A., Levy, Z., Niinobe, M., Yoshikawa, K., Arenas, E., and Fainzilber, M. (2002). The p75 neurotrophin receptor interacts with multiple MAGE proteins. J. Biol. Chem. *277*, 49101–49104.

Stem Cell Reports

Supplemental Information

Distinct Neurodegenerative Changes in an Induced Pluripotent Stem Cell Model of Frontotemporal Dementia Linked to Mutant TAU Protein

Marc Ehrlich, Anna-Lena Hallmann, Peter Reinhardt, Marcos J. Araúzo-Bravo, Sabrina Korr, Albrecht Röpke, Olympia E. Psathaki, Petra Ehling, Sven G. Meuth, Adrian L. Oblak, Jill R. Murrell, Bernardino Ghetti, Holm Zaehres, Hans R. Schöler, Jared Sterneckert, Tanja Kuhlmann, and Gunnar Hargus

Supplemental Figures

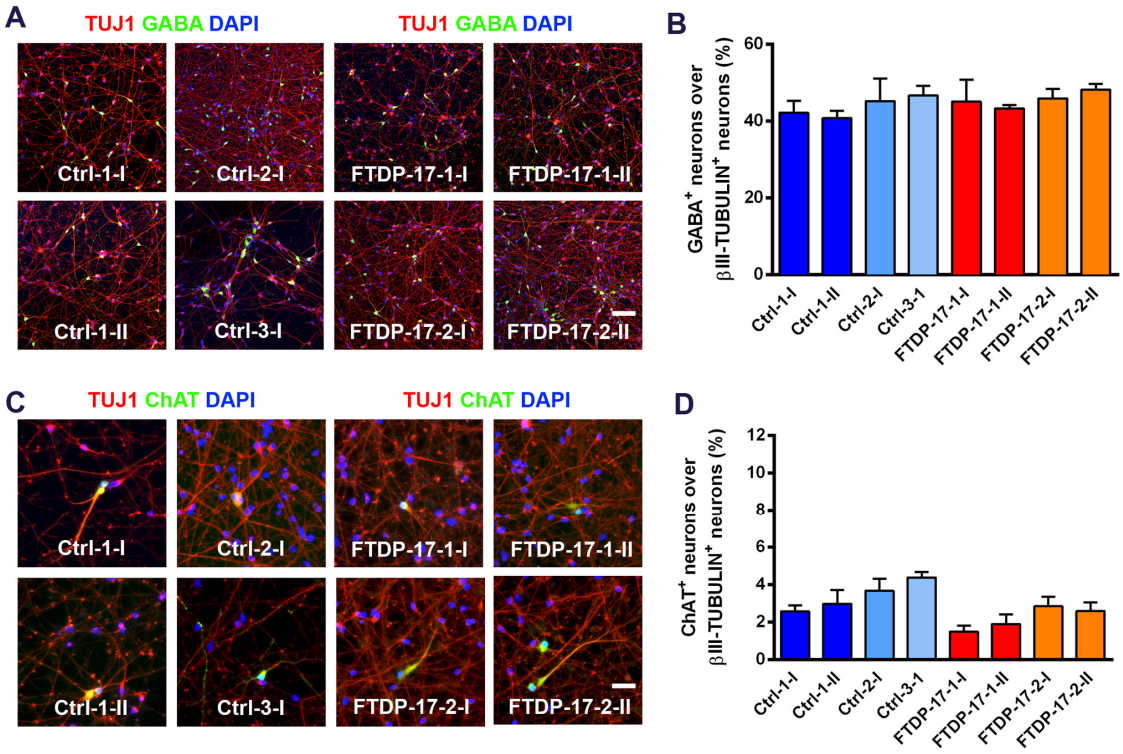

Figure S1: Differentiation of Ctrl and FTDP-17 iPS cells into mature neurons (related to Figure 2)

(**A**) Immunostainings for βIII-TUBULIN (TUJ1; red) and GABA (green) showing differentiation of Ctrl and FTDP-17 cells into GABAergic neurons. Nuclei were counterstained with DAPI (blue). Scale bar = 60 µm. **(B)** Quantification of immunostainings for βIII-TUBULIN and GABA in Ctrl and FTDP-17 neurons. Data are represented as mean of three independent differentiation experiments + SEM. **(C)** Immunostainings for βIII-TUBULIN (red) and ChAT (green) showing differentiation of Ctrl and FTDP-17 cells into cholinergic neurons. Nuclei were counterstained with DAPI (blue). Scale bar = 30 µm. **(D)** Quantification of immunostainings for βIII-TUBULIN and ChAT in Ctrl and FTDP-17 neurons. Data are represented as mean of three independent differentiation experiments + SEM.

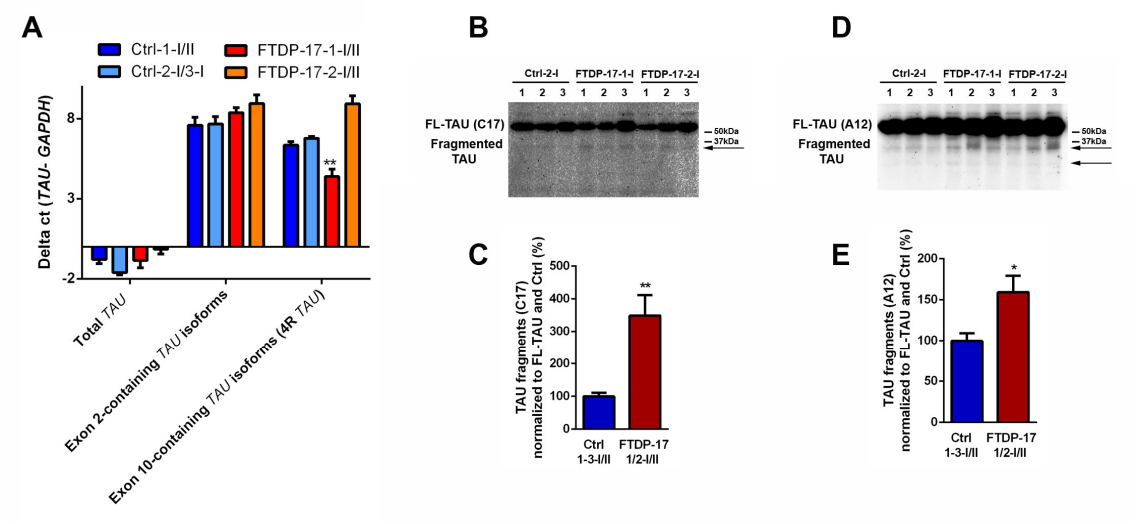

Figure S2: TAU pathology in FTDP-17 iPS cell-derived neurons (related to Figure 3).

(A) Delta ct values of qRT-PCRs on Ctrl- and FTDP-17 iPS cell-derived neurons for total *TAU*, exon 2-containing *TAU* isoforms and exon 10-containing *TAU* isoforms. Values were calculated as differences between the ct values of *TAU* (isoform) and the ct values of corresponding *GAPDH* as a housekeeping gene. Data are represented as mean of triplicates from independent differentiation experiments + SEM. One-way-ANOVA with posthoc-Tukey test was performed for statistical analysis ($^{**}p<0.01$). **(B+D)** Representative Western blot analysis on Ctrl and FTDP-17 neurons for TAU protein using the C17 (B) and A12 (D) antibodies. Independent replicates are shown for each line. **(C+E)** Quantification of TAU fragments normalized to FL-TAU and Ctrl in C17 (C) and A12 (E) Western blots. Data are presented as mean of replicates from three independent differentiation experiments per indicated lines (n=12 in C; n=11 in E) + SEM. Student's t-test was performed for statistical analysis ($^{*}p<0.05$; $^{**}p<0.01$).

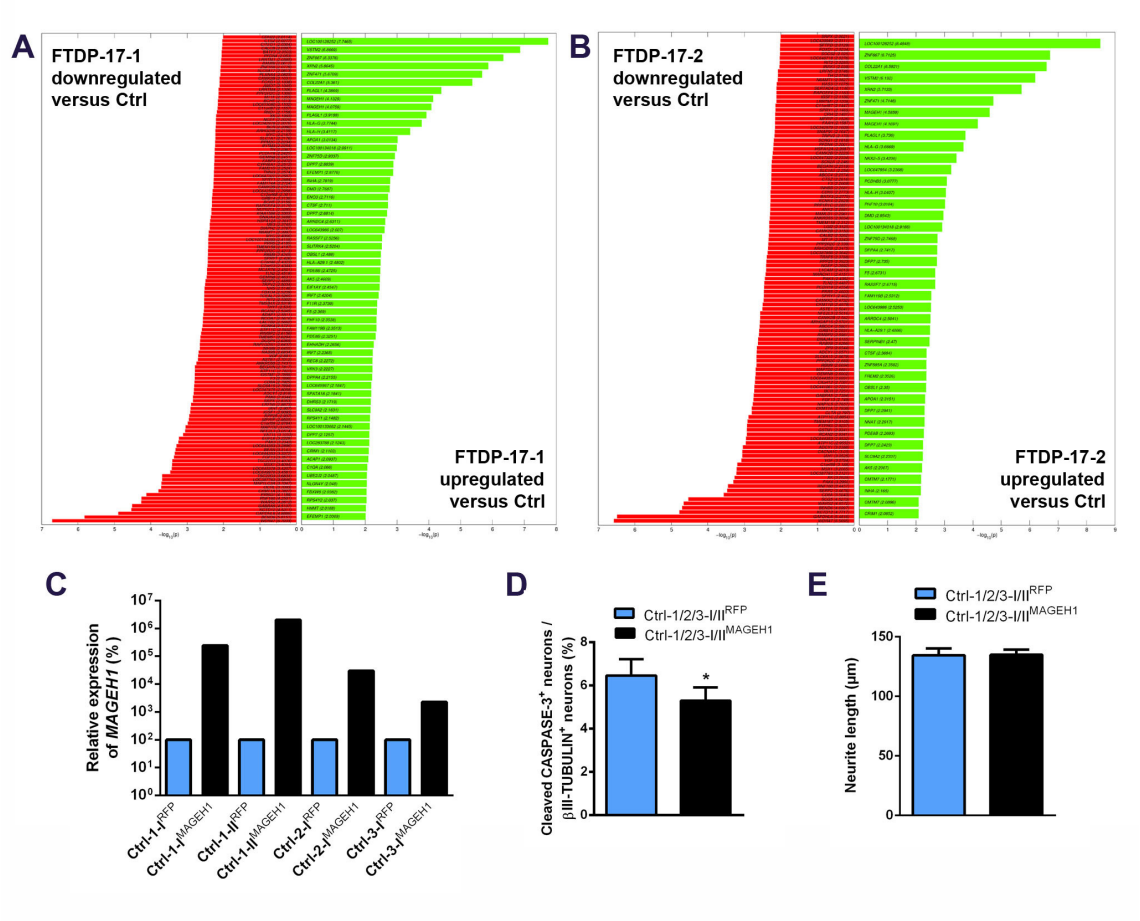

Figure S3: Differentially expressed genes in FTDP-17 neurons and *MAGEH1* overexpression in Ctrl neurons (related to Figure 5).

(A-B) Lists of differentially expressed genes (DEGs) with enhanced or reduced expression levels in FTDP-17-1 (A) and FTDP-17-2 (B) neurons and corresponding *p*-values. The bar lengths are proportional to the –log(*p*) of the DEGs. **(C)** Relative gene expression of *MAGEH1* in Ctrl-1/2/3-I/II^{MAGEH1} and Ctrl-1/2/3-I/II^{RFP} neurons. **(D)** Quantification of cleaved CASPASE-3^{+} neurons in Ctrl-1/2/3-I/II^{MAGEH1} and Ctrl-1/2/3-I/II^{RFP} neuronal cultures after 48h of rotenone treatment. At least 800 cells were counted per cell line and differentiation. **(E)** Quantification of neurite outgrowth in Ctrl-1/2/3-I/II^{MAGEH1} and Ctrl-1/2/3-I/II^{RFP} neurons 48h after plating. At least 100 neurons were measured per cell line and differentiation. Data in D and E are presented as mean of independent replicates from four different lines + SEM. Student's t-test was performed for statistical analysis ($^{*}p<0.05$).

Supplemental Tables

Table S1: Upregulated and downregulated genes in FTDP-17-1 and FTDP-17-2 neurons compared to Ctrl neurons with functional annotation (related to Figure 5)

Count	*p*-val	GSEA term link	Genes
		FTDP-17-1 upregulated	
5/152	0.00061727	EXTRACELLULAR_REGION_PART	*APOA1 C1QA DMD EFEMP1 INHA*
2/19	0.0021558	HYDRO_LYASE_ACTIVITY	*EHHADH ENO3*
2/23	0.0032029	REGULATION_OF_SECRETION	*APOA1 INHA*
3/102	0.0090825	EXTRACELLULAR_SPACE	*APOA1 C1QA INHA*
2/49	0.015058	CELL_CYCLE_ARREST_GO_0007050	*INHA PLAGL1*
2/52	0.017088	PROTEINACEOUS_EXTRACELLULAR_MATRIX	*DMD EFEMP1*
3/136	0.021052	RESPONSE_TO_EXTERNAL_STIMULUS	*F11R F5 INHA*
2/59	0.02258	GAMETE_GENERATION	*REC8 XRN2*
5/354	0.025771	BIOSYNTHETIC_PROCESS	*AK5 APOA1 DMD INHA RPS4Y1*
4/247	0.027406	CELLULAR_BIOSYNTHETIC_PROCESS	*AK5 DMD INHA RPS4Y1*
2/78	0.040793	RESPONSE_TO_WOUNDING	*F11R F5*
2/79	0.042332	SENSORY_PERCEPTION	*DHRS3 EFEMP1*
		FTDP-17-2 upregulated	
2/23	0.0025921	REGULATION_OF_SECRETION	*APOA1 INHA*
2/49	0.011854	CELL_CYCLE_ARREST_GO_0007050	*INHA PLAGL1*
3/152	0.020375	EXTRACELLULAR_REGION_PART	*APOA1 DMD INHA*
		FTDP-17-1 downregulated	
2/7	0.00080792	MONOOXYGENASE_ACTIVITY	*CYP46A1 TH*
3/29	0.001128	ANGIOGENESIS	*AMOT THY1 TNNI3*
2/11	0.0021326	CHANNEL_REGULATOR_ACTIVITY	*ADRA2A TNNI3*
4/74	0.002481	ACTIN_CYTOSKELETON_ORGANIZATION_AND_BIOGENESIS	*ADRA2A AMOT ARHGDIB RND1*
2/13	0.0030675	NEGATIVE_REGULATION_OF_CELL_ADHESION	*ARHGDIB RND1*
2/13	0.0030885	REGULATION_OF_ANGIOGENESIS	*AMOT TNNI3*
2/14	0.0036677	INTEGRIN_BINDING	*EGFL6 THY1*
3/43	0.0038277	CELLULAR_CATION_HOMEOSTASIS	*CALCB MYC THY1*
4/84	0.004137	ORGAN_MORPHOGENESIS	*AMOT MSX1 THY1 TNNI3*
2/16	0.0049455	REGULATION_OF_CELL_MIGRATION	*AMOT THY1*
4/90	0.0054186	GTPASE_REGULATOR_ACTIVITY	*ARHGDIB BCR RAPGEF4 THY1*
6/197	0.0058723	RECEPTOR_BINDING	*CALCB DIAPH2 EGFL6 FGF13 INHBB THY1*
5/155	0.0086715	CYTOSKELETON_ORGANIZATION_AND_BIOGENESIS	*ADRA2A AMOT ARHGDIB RND1 THY1*
2/22	0.0097675	HORMONE_ACTIVITY	*CALCB INHBB*
2/25	0.012662	RHO_PROTEIN_SIGNAL_TRANSDUCTION	*ADRA2A ARHGDIB*
3/81	0.024657	ENZYME_ACTIVATOR_ACTIVITY	*BCR FGF13 THY1*
2/39	0.031098	GTPASE_ACTIVATOR_ACTIVITY	*BCR THY1*
5/215	0.033959	ENZYME_REGULATOR_ACTIVITY	*ARHGDIB BCR FGF13 RAPGEF4 THY1*
3/93	0.036321	IMMUNE_RESPONSE	*ARHGDIB IFITM3 THY1*
2/42	0.036652	NEURON_DEVELOPMENT	*RND1 THY1*
2/43	0.038944	SMALL_GTPASE_REGULATOR_ACTIVITY	*ARHGDIB THY1*
5/223	0.04054	ANATOMICAL_STRUCTURE_MORPHOGENESIS	*AMOT MSX1 TH THY1 TNNI3*
3/96	0.041081	CYTOPLASMIC_VESICLE	*AMOT ARHGDIB OCRL*
2/44	0.041692	CELL_SURFACE	*SRPX THY1*

5/224	0.042267	TRANSCRIPTION_FACTOR_ACTIVITY	*BATF3 FOXD1 MYC NFE2L3 TSC22D3*

FTDP-17-2 downregulated

3/17	0.00022173	CALMODULIN_BINDING	*CACNA1C CAMKK2 RIT2*
2/5	0.00039141	NEGATIVE_REGULATION_OF_CYTOKINE_BIOSYNTHETIC_PROCESS	*INHBB SFTPD*
5/92	0.00080332	CYTOPLASMIC_MEMBRANE_BOUND_VESICLE	*ABCC4 ARHGDIB SCG5 SFTPD TMEM187*
2/7	0.00082743	HORMONE_SECRETION	*INHBB SCG5*
7/197	0.0012795	CELL_CELL_SIGNALING	*CRH FGF13 HCN2 INHBB RIT2 SCG5 SLC1A1*
4/64	0.0014954	ION_CHANNEL_ACTIVITY	*CACNA1C KCNK4 SCN2A TRPV2*
2/10	0.0018509	SECRETORY_GRANULE	*ABCC4 SCG5*
3/52	0.0069234	CATION_CHANNEL_ACTIVITY	*CACNA1C KCNK4 SCN2A*
2/22	0.0097429	REGULATION_OF_CELL_ADHESION	*ARHGDIB CDK6*
2/22	0.0098125	HORMONE_ACTIVITY	*CRH INHBB*
3/65	0.013357	CATION_TRANSPORT	*HCN2 KCNK4 SCN2A*
2/26	0.013933	VOLTAGE_GATED_CATION_CHANNEL_ACTIVITY	*CACNA1C SCN2A*
2/26	0.014035	SH3_SH2_ADAPTOR_ACTIVITY	*GRB14 SOCS2*
5/175	0.015232	SUBSTRATE_SPECIFIC_TRANSMEMBRANE_TRANSPORTER_ACTIVITY	*CACNA1C KCNK4 SCN2A SLC1A1 TRPV2*
2/35	0.026955	GTP_BINDING	*RIT2 SCG5*
2/36	0.028909	PROTEIN_PROCESSING	*CAMKK2 SCG5*

Table S2: Primary antibodies for immunocytochemistry

Antibody	Dilution	Company
mouse anti-NESTIN	1:300	R&D Systems (MAB1259)
goat anti-SOX1	1:150	R&D Systems (AF3369)
goat anti-FOXA2	1:150	Santa Cruz (sc-6554)
rabbit anti-TH	1:500	Pel Freez (P40101-150)
mouse anti-βIII-TUBULIN (TUJ1)	1:750	Covance (MMS-435P)
mouse anti-AT8	ICC 1:150 IHC 1:200	Thermo Scientific (MN1020)
rabbit anti-MAP2	1:1000	Santa Cruz (SC-20172)
rabbit anti-OCT4	1:200	Santa Cruz (SC-9081)
goat anti-NANOG	1:50	R&D Systems (AF1997)
mouse anti-SSEA-4	1:200	Millipore (SCR001/90231)
mouse anti-TRA 1-60	1:200	Millipore (SCR001/90232)
mouse anti-TRA 1-81	1:200	Millipore (SCR001/90233)
rabbit anti-HSPA5 (BiP)	1:100	Sigma (HPA038845)
rabbit anti-cleaved CASPASE-3 (Asp175)	1:1000	Cell Signaling (#9661)
goat anti-ChAT	1:300	Millipore (AB144)
rabbit anti-GABA	1:5000	Sigma (A2052)

Table S3: Primer for qRT-PCR.

*GAPDH*_for	CTG GTA AAG TGG ATA TTG TTG CCA T
*GAPDH*_rev	TGG AAT CAT ATT GGA ACA TGT AAA CC
*MAPT*_total_for	CTC GCA TGG TCA GTA AAA GCA A
*MAPT*_total_rev	GGG TTT TTG CTG GAA TCC TGG T
*MAPT*_Exon1_for	CGA AGT GAT GGA AGA TCA CG
*MAPT*_Exon2_rev	GTT CCT CAG ATC CGT CCT CA
*MAPT*_Exon2_for	TGA GGA CGG ATC TGA GGA AC
*MAPT*_Exon3_rev	TGT GGT TCC TTC TGG GAT CT
*MAPT*_Exon10_for	CCA AGT GTG GCT CAA AGG AT
*MAPT*_Exon12_rev	CCC AAT CTT CGA CTG GAC TC
*LOC100128252*_for	GCC ACT TCA TCT TGG ATG CT
*LOC100128252*_rev	GGC AAG AAT GCT GTG TCT CA
*MAGEH1*_for	GTG CCC CGG AGC AAT TTT C
*MAGEH1*_rev	CAG GCT GCA TTC CTA ACT TCC
*PAK3*_for	CAA GGG GCA TCA GGT ACT GT
*PAK3*_rev	AGA GAG CCA CCA GCC AAG TA
*SERP2*_for	GGA TGG CTA ACG AGA AGC AC
*SERP2*_rev	CAT GCC CAT CCT TAT GCT CT
*RIT2*_for	GCG GGT CCA GAG AGT ACA AG
*RIT2*_rev	GCA GTG TCC AAG ATG TCC AA
*VGF*_for	ACC ACC CTT TCC CCA ACT AC
*VGF*_rev	ATT CTC CAG CTC CTC CTG CT

Supplemental Experimental Procedures

Generation and culturing of iPS cells

Patient fibroblasts for iPS cell derivation were obtained from the Coriell Institute for Medical Research (Camden, New Jersey, USA) and had been derived from individuals carrying either the N279K mutation in exon 10 of the *MAPT* gene (FTDP-17-1; Cell repository code ND32945) or the V337M mutation in exon 12 of the *MAPT* gene (FTDP-17-2; Cell repository code ND32951). The generation of human iPS cells was performed using the lentiviral SF-OSKM-tomato vector (Warlich et al., 2011) expressing *OCT4*, *SOX2*, *KLF4* and *C-MYC* as one expression unit under the SFFV promoter as previously described (Dorn et al., 2015; Zaehres et al., 2010). Briefly, lentivirus was produced after co-transfection of packaging plasmids in 293T cells. Viral supernatant was concentrated by ultracentrifugation. Human patient-derived fibroblasts were transduced and passaged six days after transduction onto irradiated mouse embryonic fibroblast (MEF) feeders. iPS cell colonies were maintained on a layer of mitotically inactivated MEFs in human ES cell medium consisting of Knockout DMEM (Invitrogen) with 20% Knockout Serum Replacement (Invitrogen), 1 mM beta-mercaptoethanol (Invitrogen), 1% nonessential amino acids (NEAA, Invitrogen), 1% penicillin/streptomycin/glutamine (PAA), freshly supplemented with 5 ng/mL FGF2 (Peprotech). Pluripotent stem cells were split at ratios of 1:6 to 1:8 every seven days by mechanical disaggregation with 1 mg/mL collagenase IV (Invitrogen).

Characterization of iPS cells

Immunofluorescence staining of iPS cell colonies was performed using the primary antibodies OCT4 (Santa Cruz; SC-9081), NANOG (R&D Systems; AF1997), SSEA4 (Millipore; SCR001/90231), TRA 1-60 (Millipore; SCR001/90232) and TRA 1-81 (Millipore; SCR001/90233). For retroviral promoter silencing analysis, quantitative RT-PCR (qRT-PCR)

was performed using a vector-specific primer pair (*C-MYC* endo: CGT GAC CAG ATC CCG GAG TT, IRES exo: GCC TGC AAA GGG TCG CTA CA). Human iPS cells (1.5×10^6 cells/mice) were injected subcutaneously into the dorsal flank of severe combined immunodeficient mice. Eight weeks after the injection, teratomas were fixed overnight in 4% paraformaldehyde and embedded in paraffin. The sections were stained with hematoxylin and eosin dyes. For karyotype analysis, colcimid (KaryoMAX; Invitrogen) was added to a confluent culture of iPS cell-derived neural progenitor cells (NPCs) at a final concentration of 0.3 mg/mL. After three hours of incubation, cells were washed with PBS and singularized by treatment with prewarmed Trypsin-EDTA diluted in DMEM. Cells were subsequently centrifuged and the resulting cell pellet was resuspended in prewarmed KCl solution (75 mM) and incubated at room temperature for 7 minutes. Following centrifugation, cells were resuspended in ice-cold fixation solution (3:1 methanol/acetic acid) while shaking. Once fixed, cells were spun down and taken up in fresh fixative. Following 20 min at 4°C, different dilutions of cells were dropped onto glass slides (Menzel Gläser, Thermo Scientific) for analysis. Chromosomes were GTG-banded using standard procedures and metaphase spreads were analyzed on a Zeiss AxioScop and using the Cytovision software (Applied Imaging Corporation).

Generation and culturing of neural progenitor cells

NPCs were derived from iPS cells by treatment with small molecules as previously described (Hargus et al., 2014; Reinhardt et al., 2013). In short, iPS cell colonies from passages 10-15 were mechanically sectioned and enzymatically detached from MEFs. Pieces of iPS cell colonies were collected by sedimentation, resuspended in hES cell medium (without FGF) supplemented with 10 µM SB-431542 (Ascent Scientific), 1 µM dorsomorphin (Tocris), 3 µM CHIR99021 (CHIR; Axon Medchem) and 0.5 µM purmorphamine (PMA; Alexis) and subsequently cultured as embryoid bodies (EBs) in petri dishes. The medium was changed

after two days to N2B27 medium consisting in equal parts of DMEM-F12 (Invitrogen) and Neurobasal (Invitrogen) with 1:200 N2 supplement (Invitrogen), 1:100 B27 supplement lacking vitamin A (Invitrogen), 1% penicillin/streptomycin/glutamine and with the same small molecule supplements as mentioned before. On day 4, SB-431542 and dorsomorphin were withdrawn and 150 µM ascorbic acid (AA; Sigma) was added to the medium. On day 6, EBs were disintegrated into smaller pieces and plated on matrigel-coated (Matrigel, growth factor reduced, high concentration; BD Biosciences) 12-well plates (Nunc) in NPC expansion medium consisting of N2B27 supplemented with CHIR, PMA, and AA. Cells were split at ratios of 1:10 to 1:15 every five to six days.

Neuronal differentiation of neural progenitor cells

Generation of neurons from NPCs has been previously described (Hargus et al., 2014; Reinhardt et al., 2013). Briefly, singularized NPCs from passages 10 to 13 were plated on matrigel-coated plates in NPC expansion medium at a density of 2×10^5 cells per well. Two days after plating, the medium was changed to N2B27 medium supplemented with 10 ng/mL FGF8, 1 µM PMA and 200 µM AA. After six days of differentiation, the neuronal induction medium was replaced by neuronal maturation medium consisting of N2B27 with 10 ng/mL BDNF, 10 ng/mL GDNF, 10 ng/mL TGF-β3 (all from Peprotech), 200 µM AA and 500 µM dbcAMP (Sigma Aldrich). Cultures of neurons were split at ratios of 1:3 to 1:5 when confluent by detachment with a cell spatula and disintegration of the neuronal network into smaller pieces using a 1,000 µL pipette. Medium was changed every other day and cultures were analyzed after 20 days in maturation medium unless indicated otherwise.

Immunocytochemistry

For confocal microscopy, cells were cultured on matrigel-coated glass coverslips. After fixing the cells for 20 min at 4°C with 4% paraformaldehyde in PBS (Invitrogen), cells were washed

three times with 0.1% Triton X-100 (Sigma) in PBS (PBS-TX). Blocking was performed using 10% normal goat serum (NGS) in PBS-TX for 45 min at room temperature. Subsequent to blocking, coverslips were washed three times with PBS and primary antibodies were applied overnight at 4°C in 10% NGS in PBS. The next day, following three washing steps with PBS, secondary antibodies were applied for one hour at room temperature. Cells were subsequently washed three times with PBS-T (0.05% Tween-20), including a DAPI counterstaining for nuclei in the second washing step. Cells were mounted in Shandon Immu-Mount mounting medium (Fisher Scientific) and imaged on a Zeiss LSM700 confocal microscope. For quantification purposes, differentiated cells were disaggregated and seeded as single cells at a density of 6 x 10^4 cells per well in maturation medium on matrigel-coated 24-well plates. Two days after replating, cells were fixed and stained as mentioned above. Primary antibodies and their corresponding dilutions used in this study are listed in Table S2. All secondary antibodies were obtained from Invitrogen and were conjugated to AlexaFluor fluorochromes.

Quantitative RT-PCR

Total RNA was extracted from NPC-derived neurons with the RNeasy mini kit (QIAGEN) according to the manufacturer´s protocol and including an on-column DNase digest. Isolated RNA was reverse-transcribed using the High Capacity cDNA reverse Transcription Kit (Applied Biosystems). qRT-PCR was performed on an Applied Biosystems StepOne Plus real time cycler with the Power SYBR Green PCR master mix (Applied Biosystems). The melting curve of each sample was determined to ensure the specificity of the products. PCR conditions were as follows: 2 min at 50°C, 10 min at 95°C, 40 cycles of 15 sec at 95°C and 1 min at 60°C. Relative expression levels were calculated using the $2^{-2\Delta}$ method and normalized to biological reference samples and using *GAPDH* as the housekeeping gene unless otherwise noted. The primer sequences used in this study are listed in Table S3.

Electrophysiology

All measurements were conducted at room temperature in whole-cell configuration of the patch-clamp technique. Recording pipettes with resistance from 6-7 MΩ were made from borosilicate glass (GT150TF-10, Clark Electromedical Instruments, Pangbourne, UK) and filled with a solution containing (in mM): K-gluconate, 88; K_3-citrate, 20; phosphocreatine, 15; NaCl, 10; HEPES, 10; $MgCl_2$, 1; $CaCl_2$, 0.5; BAPTA, 3; Mg-ATP, 3; and Na_3-GTP, 0.5 to maintain cytosolic energy sources, buffer conditions and physiological ion concentrations. The pH was set to 7.25 with KOH and osmolality was set to 295 mOsm/kg. Cells were continuously superfused with artificial cerebrospinal fluid (ACSF) containing (in mM): NaCl, 125; KCl, 2.5; NaH_2PO_4, 1.25; $NaHCO_3$, 24; $MgSO_4$, 2; $CaCl_2$, 2; glucose, 10. The pH was adjusted to 7.35 by aeration with 95% O_2/5% CO_2 and osmolality was set to 305 mOsm/kg. Recordings were done with an EPC-10 amplifier and the Patchmaster Software (HEKA Elektronik, Lamprecht, Germany). Mean ± SD of resting membrane potential [mV] / input resistance [MΩ] / capacitance [pF] / series resistance [MΩ] were as follows: Ctrl-1-I: -65.86±3.87 / 826.57±311.38 / 14.41±7.37 / 11.1±2.59; Ctrl-2-1: -57.29±3.01 / 898.57±122.77 / 14.35±4.34 / 11.94±2.41; FTDP-17-1-I: -58.43±7.67 / 1012.0±232.03 / 17.15±5.92 / 12.11±1.54; FTDP-17-2-I: -65.75±11.64 / 710.25±200.53 / 17.52±4.87 / 12.71±3.62 . Voltage clamp mode: from a holding potential of −70 mV cells were subjected to a step protocol from -140 to 80 mV with an increment of 10 mV (duration 500 ms). Current clamp mode: action potentials were elicited with for each cell determined current steps to induce hyperpolarization in 10 mV steps from -100 to -10 mV. Tetrodotoxin (TTX, 0.5 µM, Tocris) was used to block voltage gated sodium channels. Currents under control conditions and TTX application were recorded successively from identical cells. A liquid junction potential of 12 mV was measured and taken into account when analyzing the data. Recordings were digitally analyzed using the Fitmaster software (HEKA Elektronik) and illustrated with Origin 8.5G (Origin Lab, Northampton, MA, USA).

Whole genome expression analysis

RNA samples for microarray analysis were prepared using RNeasy columns (Qiagen) with on-column DNA digestion. 300 ng of total RNA per sample was used as the input in the linear amplification protocol (Ambion), which involved the synthesis of T7-linked double-stranded cDNAs and 12 hours of *in vitro* transcription incorporating the biotin-labeled nucleotides. Purified and labeled cRNA was then hybridized for 18 hours onto HumanHT-12 v4 expression BeadChips (Illumina) following the manufacturer's instructions. After the recommended washing, the chips were stained with streptavidin-Cy3 (GE Healthcare) and scanned using the iScan reader (Illumina) and the accompanying software. The samples were exclusively hybridized as biological replicates.

Microarray data processing

The bead intensities were mapped to the corresponding gene information using BeadStudio 3.2 (Illumina) and background correction was performed using the Affymetrix Robust Multi-array Analysis (RMA) background correction model (Irizarry et al., 2003). Variance stabilization was performed using the log2 scaling, and gene expression normalization was calculated with the quantile method implemented in the lumi package of R-Bioconductor. Data post-processing and graphics were performed with in-house developed functions in MATLAB. Hierarchical clusters of genes and samples were performed with the one minus the sample correlation metric and the Unweighted Pair-Group Method using Average (UPGMA) linkage method as previously described (Kim et al., 2009)**.**

Protein analysis

Cell pellets of differentiated neurons were extracted on ice with RIPA-Buffer (Tris pH 8, NaCl, natriumdesoxycholate, NP40, SDS) containing protease inhibitors (Mini complete, Roche). Protein lysates were mixed with 6x Laemmli buffer and incubated at 95°C for 5

minutes. Denatured proteins were loaded on a 4-12% polyacrylamide gel (NuPAGE, Invitrogen) and electrophoretically separated before being transferred on a PVDF membrane. The membrane was blocked and incubated with antibodies against TAU (clone HT7, Pierce, MN1000, mouse, 1:1000; clone TAU-5, Invitrogen, AHB0042, mouse, 1:1000; clone A12, Santa Cruz, sc-166062, mouse, 1:100; clone C17, Santa Cruz, sc-1995, goat, 1:150; clone C3, Millipore, 36-017, mouse, 1:1500), BiP (Cell Signaling, C50B12, rabbit, 1:1000), p-PERK (Santa Cruz, sc-32577, rabbit, 1:1000) or PUMA (Abcam, ab9643, rabbit, 1:1000). After three washing steps, the blot was incubated with an HRP-coupled secondary antibody. The membrane was washed and then incubated with chemiluminescent HRP substrate solution (Millipore, GE). Protein expression levels were quantified by densitometric analysis using the Image Lab software (BioRad) and standardized on GAPDH (Sigma, G9545, rabbit, 1:200000) or β-ACTIN (Sigma, A5441, mouse, 1:200000).

Analysis of post-mortem tissue from FTDP-17 patients by immunohistochemistry, qRT-PCR and Western blot

Formalin fixed and paraffin-embedded sections and frozen post-mortem tissue from FTDP-17 patients (FTDP-17 A: 62 years, female, P301L; FTDP-17 B: 55 years, female, P301L; FTDP-17 C: male, N279K; FTDP-17 D: 47 years, female, N279K) and control individuals (Ctrl A: 49 years, male; Ctrl B: 80 years, female) were obtained from the Department of Pathology and Laboratory Medicine (Dr. Bernardino Ghetti´s Lab) at Indiana University. Immunohistochemistry was performed on de-paraffinized and rehydrated sections on an automated staining system (Auto Stainer Link 48, DAKO). Sections were counterstained with haematoxylin before being dehydrated and covered in Eukitt. Antibodies employed for immunohistochemistry were anti-AT8 (no pretreatment; 1:200) and anti-BiP (pretreatment with target retrieval solution, pH 6.1; 1:100).

For qRT-PCR, RNA was isolated from frozen midbrain tissue specimen using Maxwells 16 LEV simplyRNA Tissue Kit on Maxwell 16 Instrument (Promega). Isolated RNA was transcribed into cDNA using the High Capacity cDNA reverse Transcription Kit (Applied Biosystems) and qRT-PCR was performed on an Applied Biosystems StepOne Plus real time cycler with the Power SYBR Green PCR master mix (Applied Biosystems).

For Western blot analysis, cell lysates were generated from frozen midbrain tissue specimen by mechanical grinding of the tissue followed by homogenization with an ultra turrax. SDS sample buffer was added to samples holding 40 µg of total protein followed by incubation at 95°C for 5 min. Protein samples were separated in 10% polyacrylamide/SDS gels and subsequently blotted onto PVDF membranes. Primary antibodies employed for Western blotting were anti-BiP (Cell Signaling, rabbit, 1:1000) and anti-GAPDH (Sigma, rabbit, 1:200000). The HRP-labeled antibody anti-rabbit (Cell Signaling, 1:5000) was used as secondary antibody. Visualization of the proteins was achieved by incubation with chemiluminescent HRP substrate solution (Millipore, GE).

Knockdown of *MAGEH1*

Gene knockdown of *MAGEH1* was performed using lentiviral particles containing a mix of 5 different Mission® shRNA (Sigma) constructs encoding *MAGEH1*-specific shRNAs. Control cell populations were prepared using scrambled Mission® shRNA (Sigma) lentiviral particles. Virus particle production and transduction of NPCs was done as previously described (Hargus et al., 2014). Cells that had not been transduced were removed prior to neuronal differentiation through puromycin (5 µg/ml) selection for one week.

Lentiviral expression of *MAGEH1*

MAGEH1 was cloned from cDNA derived from FTDP-17-1 neurons using gene specific primers with attb gateway cloning sites attached (for: 5´-

GGGGACAAGTTTGTACAAAAAAGCAGGCTTCACCATGCCTCGGGGACGAAAGAGTCGG- 3′, rev: 5′-GGGGACCACTTTGTACAAGAAAGCTGGGTTTTAAGGGGCGGAATAACCCCTAGCA-3′). PCR was performed using Phusion polymerase (NEB) and PCR conditions were set according to the manufacturer's recommendations. *MAGEH1* sequence integrity was verified by sequencing. For overexpression in NPCs, the PCR product was introduced into the pLEX_307 plasmid using the Gateway cloning technique. The expression vector pLEX_307 was a gift from David Root (Addgene plasmid # 41392). Production of the lentiviral pLEX_307 vector expressing either MAGEH1 or dtTomato (red fluorescent protein) and transduction of NPCs was performed as previously described (Hargus et al., 2014). Cells that had not been transduced were removed prior to neuronal differentiation through puromycin (5 μg/ml) selection for one week.

Supplemental References

Dorn, I., Klich, K., Arauzo-Bravo, M.J., Radstaak, M., Santourlidis, S., Ghanjati, F., Radke, T.F., Psathaki, O.E., Hargus, G., Kramer, J.*, et al.* (2015). Erythroid differentiation of human induced pluripotent stem cells is independent of donor cell type of origin. Haematologica *100*, 32-41.

Hargus, G., Ehrlich, M., Arauzo-Bravo, M.J., Hemmer, K., Hallmann, A.L., Reinhardt, P., Kim, K.P., Adachi, K., Santourlidis, S., Ghanjati, F.*, et al.* (2014). Origin-dependent neural cell identities in differentiated human iPSCs in vitro and after transplantation into the mouse brain. Cell Rep *8*, 1697-1703.

Kim, J.B., Sebastiano, V., Wu, G., Arauzo-Bravo, M.J., Sasse, P., Gentile, L., Ko, K., Ruau, D., Ehrich, M., van den Boom, D.*, et al.* (2009). Oct4-induced pluripotency in adult neural stem cells. Cell *136*, 411-419.

Reinhardt, P., Glatza, M., Hemmer, K., Tsytsyura, Y., Thiel, C.S., Hoing, S., Moritz, S., Parga, J.A., Wagner, L., Bruder, J.M.*, et al.* (2013). Derivation and expansion using only small molecules of human neural progenitors for neurodegenerative disease modeling. PLoS One *8*, e59252.

Warlich, E., Kuehle, J., Cantz, T., Brugman, M.H., Maetzig, T., Galla, M., Filipczyk, A.A., Halle, S., Klump, H., Scholer, H.R.*, et al.* (2011). Lentiviral vector design and imaging approaches to visualize the early stages of cellular reprogramming. Mol Ther *19*, 782-789.

Zaehres, H., Kogler, G., Arauzo-Bravo, M.J., Bleidissel, M., Santourlidis, S., Weinhold, S., Greber, B., Kim, J.B., Buchheiser, A., Liedtke, S.*, et al.* (2010). Induction of pluripotency in human cord blood unrestricted somatic stem cells. Exp Hematol *38*, 809-818, 818 e801-802.